Eurasian Chem.-Technol. J. 27 (2025) 45–70
The journal of the Institute of Combustion Problems https://ect-journal.kz

https://doi.org/10.18321/ectj1655

Experimental and Surface Evaluation of Zinc Electroplating Efficiency and Corrosion Inhibition Effects of *Centaurea napifolia* Extracts

Habiba Soltani[1,2], Karima Hanini[2,3], Merzoug Benahmed[3,5], Sameh Boudiba[2], Louiza Boudiba[2], Alfred Ngenge Tamfu[4]*, Amar Zellagui[5], and Salah Akkal[6]

[1]*Laboratory of Organic Materials and Heterochemistry (LOMH), Echahid Cheikh Larbi Tebessi University, Constantine Road, 12002, Tebessa, Algeria*
[2]*Laboratory of Applied Chemistry and Renewable Energies (LACRE), Echahid Cheikh Larbi Tebessi University, Constantine Road, 12002, Tebessa, Algeria*
[3]*Laboratory of Bioactive Molecules and Applications (LBMA), Echahid Cheikh Larbi Tebessi University, Constantine Road, 12002, Tebessa, Algeria*
[4]*Department of Chemical Engineering, School of Chemical Engineering and Mineral Industries, University of Ngaoundere, 454 Ngaoundere, Cameroon*
[5]*Laboratory of Biomolecules and Plant Breeding (LBPB), Larbi Ben M'hidi University, 04000 Oum El Bouaghi, Algeria*
[6]*Laboratory of Phytochemistry, Physicochemical and Biological Analyzes (LPPBA), Mentouri University, Ain el Bey Road, 25000 Constantine, Algeria*

Article info

Received:
31 October 2024

Received in revised form:
15 December 2024

Accepted:
10 January 2025

Keywords:
Centaurea napifolia
Zinc electroplating
Additives
Corrosion inhibitor
Electrochemical impedance
Surface morphology

ABSTRACT

This study introduces *Centaurea napifolia* as a novel multifunctional corrosion inhibitor and a zinc-electroplating additive previously unexplored in the field. Hydro-methanolic, methylene dichloride, ethyl acetate, and *n*-butanol extracts were investigated for their dual functionality: inhibiting corrosion of carbon steel and improving the performance of zinc electrodeposition on mild steel. Using techniques such as potentiodynamic polarization, gravimetric methods, electrochemical impedance spectroscopy, scanning electron microscopy/energy dispersive spectroscopy, and profilometry, significant improvements in brightness, corrosion resistance, coating quality, and adhesiveness have been found. Notably, adding 3.2 g/l butanolic extract achieved an optimal corrosion rate of 0.038 mm/y, a substantial improvement over unplated mild steel and plated samples without additives, and reduced current density from 0.3235 mA/cm² to as low as 0.0033 mA/cm². These extracts showed effective inhibition against carbon steel corrosion in acidic environments with efficiencies up to 82%, following the Langmuir isotherm model with physical adsorption being spontaneous and exothermic, highlighting the potential of *Centaurea napifolia* extracts as eco-friendly alternatives for metal protection. These findings translate to significant economic opportunities for industries reliant on metal protection systems by offering eco-friendly alternatives that could reduce environmental impact while enhancing the durability of metal components used for practical or industrial applications.

1. Introduction

Metals have accompanied mankind since ancient times [1] due to their use in almost every aspect of our lives. Among these metals, steel stands out as an ever-evolving material, offering a wide range of properties, such as durability and strength, that can meet ever-changing requirements, making it a popular choice for many various applications, especially in industry and engineering construction [2]. However, steel possesses a drawback: it is prone to rusting upon exposure to its surroundings [3]. This inevitable and undesirable phenomenon not only

*Corresponding author.
E-mail address: macntamfu@yahoo.co.uk

has economic implications but also jeopardizes our health and environment [4-7]. For these reasons and to mitigate or avoid the corrosion of metallic materials, many techniques are employed, such as electroplating and corrosion inhibitors [8]. For a better understanding, electroplating is a process where a direct current is used to reduce the cations of a desired material in an electrolytic solution, resulting in a thin metallic coating on the substrate surface [9-11]. Among different electroplating methods, zinc plating is the most commonly employed technique [12-14], particularly for protecting steel against corrosion. This method possesses sacrificial properties that protect the coated metal, even if the deposit is porous. Zinc plating is also preferred due to its low cost and the simplicity of the implementation process [15-17]. Corrosion inhibitors are chemicals that have heteroatoms (S, O, N…), multiple bonds, and aromatic rings in their structures [18, 19]. They slow down corrosion when added in small amounts to a corrosive environment [20], like that found in pickling [21] or other acidic processes [22, 23].

With the increasing awareness of environmental and human health concerns, researchers are placing greater emphasis on green chemistry. This approach encourages the utilization of natural products, particularly plants, as a valuable resource due to their availability, biodegradability, and abundance of secondary metabolites like polyphenols, alkaloids, tannins, and so forth. These valuable compounds can be easily and affordably extracted using straightforward methods [24-27]. The utilization of plant extracts extended beyond the realm of medicine [28-30], encompassing various domains, such as protecting metals and alloys against corrosion [31]. In this context, plant extracts have shown very good performance as additives [19, 32-36] in electroplating baths to enhance the quality of plating (roughness, porosity, brightness, and corrosion resistance) [9]. They have proven to be valuable inhibitors in acidic solutions, effectively reducing the corrosion rate [18, 37, 38].

Despite their potential benefits, there is a notable lack of comprehensive studies exploring the dual role of plant extracts as both effective corrosion inhibitors and performance-enhancing additives. Specifically, *Centaurea napifolia* extracts have remained unexplored for their potential to inhibit corrosion and enhance the performance of zinc deposition. This study aims to fill this gap by investigating Centaurea napifolia, an annual plant rich in polyphenols and sesquiterpene lactones [39-41]. The investigation focuses on evaluating its effectiveness as a corrosion inhibitor for industrial carbon steel (API 5L-X60) and its potential as additives in performance-enhancing zinc electroplating baths for industrial mild steel (E24-2). By addressing this oversight, valuable insights can be gained into optimizing plant extracts to improve both the durability of carbon steel through enhanced corrosion resistance and the quality of zinc coatings on mild steel for protective across industries.

2. Experimental

2.1 Plant extracts

Aerial parts of *Centaurea napifolia* were collected over its flowering period in Grarem, Mila, Algeria, on May 5, 2020. Dr. ZELLAGUI Amar from the Biology Department of Larbi Ben M'hidi University in Oum El Bouaghi, Algeria, identified specimens. A voucher specimen was deposited in the Laboratory of Biomolecules and Plant Breeding, University of Larbi Ben M'hidi (Oum El Bouaghi, Algeria, voucher number ZA 66). The collection took place under consistent spring weather conditions; however, future studies should consider evaluating how seasonal variations might affect extract properties. The dried aerial parts were cut into small pieces and then immersed in a hydromethanolic mixture (7/3) for 24 hours. The mixture was filtered, and the filtrate was evaporated to dryness. The operation was repeated three times. The residue was dissolved in boiling water and kept overnight at room temperature, allowing the elimination of chlorophyll and other impurities. The filtered mixture was split into two parts. To get HME, the first part is evaporated in a vacuum. The second part is then extracted with three organic solvents of increasing polarity, starting with methylene dichloride, then ethyl acetate, and ending with *n*-butanol. The obtained organic phases were then concentrated to dryness to get MDE, EAE, and BE, respectively [26, 42].

2.2 Electrodeposition additives

2.2.1 Electrodeposition bath

The electrodeposition bath consists of boric acid H_3BO_3 (20 g/L), which is used as a buffer and a fluxing agent to avoid the formation of zinc hydroxide. Zinc dichloride, $ZnCl_2$ (65 g/l), was used to maintain the Zn level in the bath steady by dissolving Zn anodes, which substitute the $ZnCl_2$ contained in the solution. Potassium chloride KCl (200 g/l) provides the chloride content, which helps to enhance the

conductivity of the solution. Different concentrations of *Centaurea napifolia* extracts were tested as additives [33, 36].

2.2.2 Materials

Flat mild steel (MS) (E24-2), with a composition of (wt%): 0.17% C, 0.6% Mn, 0.035% P, 0.035% S, 0.04% Si, 0.02-0.05% Al, 0.01% N, and the remainder Fe, are supplied from the production unit of the «ANABIB» gas pipes of Tebessa-Algeria. Specimens were coated with epoxy resin, leaving an exposed surface area of 2 cm x 4 cm. The exposed surface area of specimens during electrochemical and corrosion tests was typically 2 cm x 2 cm. The substrates were abraded using different grades of emery paper, cleaned with acetone, rinsed with distilled water, and air-dried before being used for further experiments.

2.2.3 Experimental conditions

The zinc electroplating of the steel surface (SS) was performed by immersing in electroplating baths the substrate, which represents the cathodic part of the DC supply, and the pure zinc plate (99.91%), forms the anodic part, leaving a distance of 1 cm between them. After several tests, the best experimental conditions were obtained for a current value of 0.04 A, a pH=5, and a plating time of 30 min [43, 44]. After each plating experiment, the coated plates were taken off, cleaned with distilled water, air-dried, and weighed before and after the electroplating process to determine the weight of the zinc deposit.

2.2.4 Adhesion test

The adhesion of the zinc coating to the steel substrate was tested using adhesive tape attached to the surface after an 'X' letter engraved on the film, which was then strongly removed. Any zinc stripping from the plated steel surface will be visually seen [45].

2.2.5 Surface brightness

To measure the gloss of the samples, a Poly Gloss device was used, The measurements were taken at angles of 20°, 60°, and 85°, consistent with ASTM D523 and DIN EN ISO 2813 recommendations, and an average value was obtained from three measurements for each coating.

2.2.6 Electrochemical measurements

All electrochemical experiments were realized at room temperature with a potentiostat-galvanostat PGZ 301 radiometer related to the software "Voltamaster 4". A platinum wire was used as a counter electrode, a saturated calomel electrode (SCE) as a reference electrode, and the coated samples as the working electrode. Before each measurement, the coated samples were immersed in seawater at open circuit potential (OCP) to ensure its steady state. Electrochemical impedance spectroscopy (EIS) was carried out on each coated sample over a frequency range of 100 KHz-10 mHz with a signal amplitude perturbation of 10 mV.

The potentiodynamic polarization measurements were made in the potential range of ±250 mV at a sweep rate of 1 mV/s.

2.2.7 Scanning electron microscopy with energy dispersive spectroscopy (SEM/EDS) for zinc electroplating

The surface morphology and chemical composition of the deposited layers were studied using a scanning electron microscope with energy-dispersive spectroscopy (Thermo scientific).

2.2.8 Profilometer analysis

To evaluate the surface roughness of deposited layers, an optical profilometer (AltiSurf 520) was used. The instrument is non-contact and does not damage the surface, offering high-resolution surface analysis and providing 3D surface morphology and its amplitude parameters.

2.3 Corrosion Inhibitors

2.3.1 Electrolytic solution and materials

The aggressive solution consists of 1M HCl (prepared by dilution of an analytical-grade HCl with distilled water), with the addition of different concentrations of HME, MDE, EAE, and BE. All experiments were performed on CS specimens with composition in weight percentage as follows: C, 0.26; Mn, 1.35; P, 0.03; S, 0.03; and the balance Fe.

2.3.2 Electrochemical measurements

The electrochemical experiments were conducted at room temperature, using an Origaflex 500 potentiostat-galvanostat monitored by Origamaster 5.

A platinum wire was used as a counter electrode, a saturated calomel electrode (SCE) was used as a reference electrode, and API 5L-X 60 steel with a surface area of 1 cm^2 was used as the working electrode. Before each measurement, the working electrode was immersed for 30 min at OCP. The EIS experiments were carried out over a frequency range of 100 KHz to 100 MHz with a signal amplitude perturbation of 10 mV. The inhibition efficiency η_R (%) was calculated using Eq. 1 [46]:

$$\eta_R(\%) = \frac{R_{ct} - R_{ct}^{o}}{R_{ct}} \cdot 100 \quad (1)$$

where R_{ct}° and R_{ct} are charge transfer resistances in the absence and presence of the inhibitor, respectively.

The potentiodynamic polarization measurements were made in the potential range of ±250 mV at a sweep rate of 1 mV/s. The inhibition efficiency η_P (%) was calculated using the following Eq. 2 [47]:

$$\eta_P(\%) = \frac{i_{corr}^{o} - i_{corr}}{i_{corr}^{o}} \cdot 100 \quad (2)$$

where i_{corr}° and i_{corr} are the corrosion current densities values in the absence and presence of the inhibitor, respectively.

2.3.3 Weight loss studies

Weight loss allows us to estimate the corrosion rate and deduce the inhibitory efficiency for each tested extract concentration. The clean samples were weighed before and after being suspended in an aerated stagnant electrolytic solution for two hours at different temperatures, and the difference in weights was determined and used to calculate the corrosion rate and inhibition efficiency (η_w (%)) using Eqs. 3-4, respectively [4, 48]:

$$CR = \frac{W}{At} \quad (3)$$

$$\eta_W(\%) = \frac{CR^{o} - CR}{CR^{o}} \cdot 100 \quad (4)$$

where w is the average weight loss, A is the total area of one carbon steel specimen, and t is the immersion time, CR° and CR are the corrosion rates in the absence and presence of inhibitors, respectively.

2.3.4 Scanning electron microscopy with energy dispersive spectroscopy (SEM/EDS) for corrosion inhibition

The surface analysis of the CS specimens was performed using SEM combined with EDS after immersion in 1M HCl solution without and with the addition of optimal concentrations of HME, MDE, EAE, and BE at 293 K for 2 hours.

3. Results and discussion

3.1 Electrodeposition Additives

3.1.1 Potentiodynamic polarization measurements

Figure 1 represents the potentiodynamic polarization curves of samples coated in the absence and presence of different concentrations of HME, EAE, and BE.

As evident in Fig. 1, samples plated in the presence of HME, EAE, and BE exhibited more cathodic abandonment potentials and lower current densities. This suggests that these additives influence the electrochemical properties of the samples post-deposition. The reduced current densities associated with these samples may indicate a decrease in reactivity towards corrosive species present in seawater, potentially leading to enhanced durability and improved protection against corrosion [19].

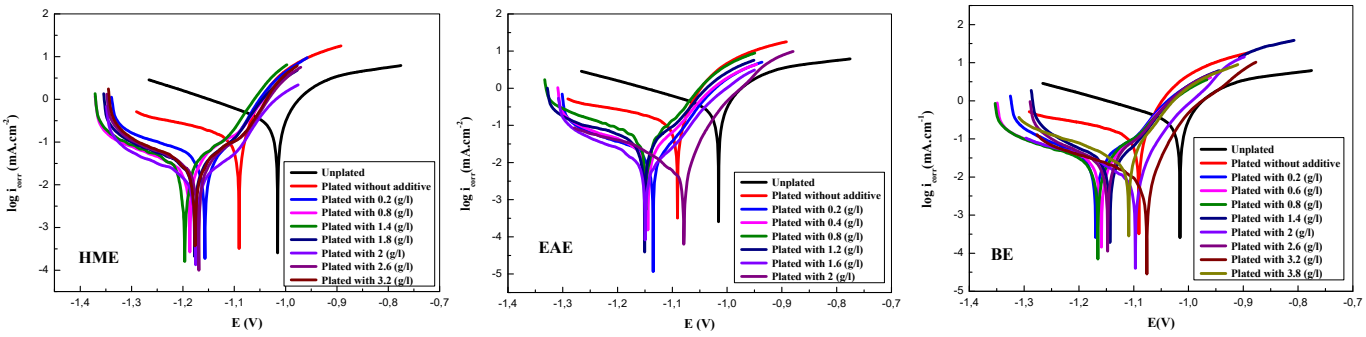

Fig. 1. Potentiodynamic polarization curves for unplated and zinc-plated substrates without and with different concentrations of additives.

Table 1. Potentiodynamic polarization parameters for unplated and zinc-plated substrates without and with different concentrations of additives

Extract	C (g/l)	$-E_{corr}$ (V/SCE)	i_{corr} (mA/cm²)	β_a (mV/Dec¹)	$-\beta_c$ (mV/Dec¹)	R_p (Ω cm²)	CR (mm/y)	P (%)	η_P (%)
MS		1015.5	0.3235	95.4	264.8	62.2	3.78300	/	/
Without extract		1090.5	0.0972	86.9	264.4	148.82	1.13700	0.05728	/
HME	0.2	1157.1	0.0297	69.0	191.9	581.27	0.34698	0.00094	69.44
	0.8	1186.3	0.0141	76.9	159.5	673.89	0.16549	0.00055	85.49
	1.4	1177.2	0.0132	70.4	122.5	1300.00	0.15410	0.00024	86.41
	1.8	1176.9	0.0134	72.5	136.3	657.65	0.15660	0.00056	86.21
	2	1174.8	0.0055	70.1	151.4	1420.00	0.06395	0.00023	94.34
	2.6	1169.1	0.0125	72.3	121.2	917.34	0.14590	0.00051	87.14
	3.2	1176.3	0.0129	70.4	125.0	759.55	0.15030	0.00042	86.73
EAE	0.2	1133.6	0.0127	59.4	129.6	841.87	0.14810	0.00076	86.93
	0.4	1144.7	0.0187	68.4	173.2	758.27	0.21920	0.00106	80.76
	0.8	1148.5	0.0283	63.7	150.9	557.34	0.32740	0.00091	70.88
	1.2	1150.5	0.0219	68.0	169.3	606.84	0.25590	0.00106	77.47
	1.6	1149.3	0.0078	68.0	131.1	1850.00	0.09110	0.00036	91.97
	2	1078.8	0.0163	60.3	306.6	2190.00	0.18845	0.00253	83.23
BE	0.2	1169.2	0.0212	79.3	139.7	709.99	0.24510	0.00101	78.18
	0.6	1159.0	0.0163	74.7	164.2	942.63	0.19100	0.00079	83.23
	0.8	1165.3	0.0145	75.0	203.9	934.16	0.16960	0.00067	85.08
	1.4	1143.4	0.0240	68.2	150.3	668.22	0.28030	0.00124	75.31
	2	1096.9	0.0073	53.1	173.5	1560.00	0.08486	0.00116	92.48
	2.6	1147.6	0.0122	58.7	72.8	722.99	0.14300	0.00048	87.45
	3.2	1075.9	0.0033	50.6	132.5	2100.00	0.03829	0.00189	96.60
	3.8	1109.1	0.0178	71.1	158.0	476.66	0.20800	0.00629	81.69

The corrosion potential E_{corr}, corrosion current density i_{corr}, anodic Tafel slope β_a, cathodic Tafel slope β_c, the resistance of polarization R_p, corrosion rate CR, the porosity P, which is calculated according to Eq. 5 and the η_P (%) calculated according to Eq. 6 [49] are illustrated in Table 1.

$$P = \frac{R_{ps}}{R_p} 10^{-(\Delta E_{corr}/\beta_a)} \quad (5)$$

where: R_{ps} and R_p are the polarization resistances of unplated and coated substrates, respectively. ΔE_{corr} is the potential difference between the unplated substrate and the coated substrate.

$$\eta_P(\%) = \frac{i^o_{corr} - i_{corr}}{i^o_{corr}} 100 \quad (6)$$

where i_{corr}° and i_{corr} are the current densities for the samples plated without and with the addition of different concentrations of additives, respectively.

From the results illustrated in Table 1, it is noticed that the values of i_{corr}, CR, and P for plated samples in the presence of additives, compared to those obtained in their absence are lower. This indicates that the presence of extracts in the electroplating bath enhances deposit quality by improving the coating stability and durability while reducing vulnerability to corrosion, the extracts influence crystal formation and surface morphology by inhibiting unwanted crystal growth directions through adsorption onto the plated surface, often integrating into the deposit itself [36, 50]. However, there was a non-linear relationship between corrosion current density and additive concentration in the electroplating bath. This suggests that each electroplating process has an optimal additive concentration that yields the highest deposit quality [36]. This non-linearity maybe arises from microstructural modifications imparted by additives during electrodeposition. At optimal concentrations, additives form a coherent structure

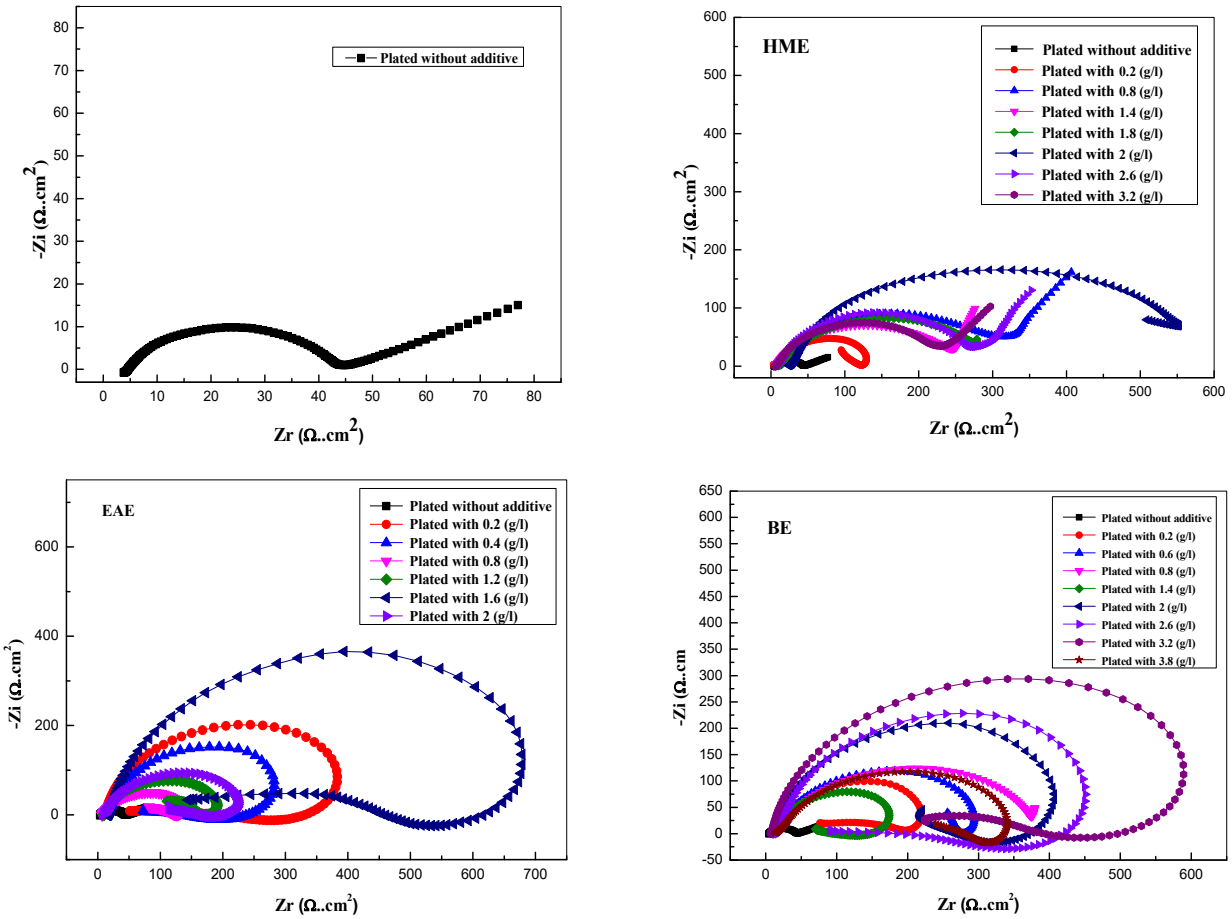

Fig. 2. Electrochemical impedance plots of coated steels without and with the addition of different concentrations of additives.

that suppresses defects nucleation (e.g., voids, dislocations) and stabilizes passive films, but deviations lead to microstructural heterogeneity and reactive sites. During potentiodynamic polarization in seawater, chloride ions exploit these sites, accelerating passive film breakdown and contributing to the observed non-linear trends in corrosion behavior. The cathodic shift at 2.6 g/l compared to 2, 3.2, and 3.8 g/l may be attributed to the optimal extract adsorption during electroplating coupled with residual adsorption post-plating, which maximizes the suppression of cathodic reactions (oxygen reduction). Notably, using 3.2 g/l of BE resulted in a remarkable inhibition efficiency of 96.60%. These findings are consistent with those observed for other plant-based additives, such as *Pyracantha coccinea* extracts [36].

3.1.2 EIS measurements

It is to highlight that the EIS is a powerful and a non-destructive technique that may provide information on the effects of additives [51, 52].

Figure 2 provides Nyquist plots of coated specimens. As illustrated in Fig. 2, the addition of all investigated extracts used as additives increase the capacitive loop diameter, indicating that the substrates coated in the presence of these additives were more resistant to corrosion.

From the Nyquist plots, two cases can be distinguished: for the samples plated in the presence of all EAE concentrations (0.2, 2 g/l) of the HME and all BE concentrations, with the exception of 0.8 g/l, the impedance spectra consist of one capacitive loop at high frequencies followed by one inductive loop at low frequencies. According to the reported literature [53], the inductive loop may be linked to the stability of the intermediate layer by dissolution reaction products adsorbed on the surface electrode. On the other hand, the first loop is usually attributed to the charge transfer through the double layer for the corrosion reaction. For samples that were plated without and in the presence of additives, the impedance diagram shows a capacitive loop for high frequencies, which is related to charging transfer, followed by a straight line for low frequencies due to the Warburg impedance, indicating that the coating is corroding significantly due to the diffusion effect [54].

Table 2. Electrochemical impedance parameters of coated steels without and with varying additive concentrations

	C (g/l)	R_{tc}. (Ω.cm²)	C_{dl} (µF.cm^{-2})	η_R (%)
Without extract	0	39.76	179.300	/
HME	0.2	134.45	53.030	70.42
	0.8	327.99	172.740	87.87
	1.4	255.50	87.206	84.43
	1.8	296.21	120.350	86.58
	2	576.44	43.623	93.10
	2.6	278.16	101.840	85.70
	3.2	238.04	133.710	83.29
EAE	0.2	387.93	12.964	89.75
	0.4	293.34	19.315	86.44
	0.8	137.23	57.987	71.02
	1.2	193.71	25.962	79.47
	1.6	695.46	11.442	94.28
	2	228.47	13.931	82.59
BE	0.2	225.98	25.071	82.40
	0.6	293.01	24.330	86.43
	0.8	379.55	41.932	89.52
	1.4	180.31	17.652	77.94
	2	423.34	16.842	90.60
	2.6	461.84	12.268	91.39
	3.2	627.37	7.103	93.66
	3.8	341.57	16.587	88.35

Table 2 summarizes the EIS parameters of coated steels without and with varied additive concentrations, and the η_R (%) values were determined using Eq. 7 [19]:

$$\eta_R(\%) = \frac{R_{ct}^{o} - R_{ct}}{R_{ct}^{o}} 100 \quad (7)$$

where R_{ct}° and R_{ct} are the charge transfer resistances for samples plated in the absence and presence of different concentrations of the studied extracts, respectively.

The values of R_{ct} for the samples coated in the presence of various amounts of extracts were higher compared to the sample coated in their absence, indicating a decrease in the corrosion rate, as can be seen in Table 2. Moreover, a decrease in C_{dl} values for the coated specimens in the presence of additives compared to that obtained without them were noticed. The highest inhibition efficiency noted for the concentration of 1.6 g/l of EAE was 94.28%, which fits well with the values obtained from potentiodynamic polarization parameters.

3.1.3. Quality of electrodeposited zinc

Brightness, adhesion strength, and thickness were utilized to assess the quality of the plated deposit. The thickness was determined using Faraday's law according to Eq. 8.

$$T = \frac{m}{\rho.S} \cdot 10000 \quad (8)$$

where T is the thickness, m is the deposited mass, ρ the zinc density, and S is the deposit area. The constant 10000 is used to convert the unit cm to µm.

Table 3 displays the acquired results, which show that all tested thickness values were within the standard norms established by ASTM rules A879 and B633 [55, 56].

According to the obtained results, the mass of zinc deposited in the presence of the additive was a more significant than in its absence. Furthermore, the deposited zinc has a firm adherence, without regularity for all evaluated concentrations. We can also see that samples plated without and with (0.8,1.2, 1.6 and 2 g/L) of EAE, and (0.8, 2, 3.2, and 3.8 g/L) of

Table 3. Deposited zinc layer's mass, thickness, adhesion strength, and brightness when various concentrations of HME, EAE, and BE are used as additives

Extract	C(g/l)	Deposited mass (g)	Thickness (μm)	Adhesion	Brightness (GU)
Without extract	/	0.0217	11.26	+	18.2 Matte
HME	0.2	0.0318	13.29	+++	49.8 Semi bright
	0.8	0.0326	13.76	++	88 Bright
	1.4	0.0327	14.18	+++	82.5 Bright
	1.8	0.0291	12.28	+++	94.7 Bright
	2	0.0289	12.49	+++	37.5 Semi bright
	2.6	0.0334	14.07	+++	34.8 Semi bright
	3.2	0.0271	11.41	+++	76.9 Bright
EAE	0.2	0.0371	15.65	++	69.5 Bright
	0.4	0.0356	15.21	+++	40.2 Semi bright
	0.8	0.0304	13.05	++	21.1 Matte
	1.2	0.0368	15.45	+++	13.2 Matte
	1.6	0.0339	14.51	+++	16.4 Matte
	2	0.0388	16.79	+++	12.5 Matte
BE	0.2	0.0324	14.21	++	49.4 Semi bright
	0.6	0.0395	17.45	++	50.9 Semi bright
	0.8	0.0325	14.24	+++	27.9 Matte
	1.4	0.0369	16.82	+++	37.2 Semi bright
	2	0.0235	10.57	+++	18.8 Matte
	2.6	0.0358	15.95	+++	36.4 Semi bright
	3.2	0.0329	14.53	++	19.5 Matte
	3.8	0.0299	12.98	++	16.1 Matte

BE were matte. The semi-gloss appearance was seen in samples coated with (0.2, 2, and 2.6 g/L) HME, (0.4 g/L) EAE, and (0.2, 0.6, 1.4, and 2.6 g/L) BE. Ultimately, in the presence of (0.8, 1.4, 1.8, and 3.2 g/L) HME, and (0.2 g/L) EAE, the brightness appeared [57, 58]. This observation can be attributed to two plausible mechanisms. Firstly, the adsorption of the additive onto the steel surface may lead to a partial coating, thereby blocking active sites and reducing the nucleation rate. Secondly, it is possible that the additive forms a complex with one of the electroactive species present in the solution. This complexation introduces a new kinetic constant at the dissociation step preceding the redox reaction involving electroactive species at the electrode surface [36].

3.1.4 Scanning electron microscopy with energy dispersive spectroscopy (SEM/EDS) for zinc electroplating

SEM was used to analyze the surface morphology of Zn electrodeposited MS samples with and without plant extract additives. Additionally, EDS analysis was conducted to determine the composition of the plated metal surface. The results are presented in Fig. 3.

Figure 3 shows the SEM image of the plated MS surfaces without and with the addition of HME, EAE, and BE in the chloride bath. The obtained results revealed uneven dendritic crystal growth with low microscopic porosity in some places. Furthermore, there was a mixture of coarse and fine particles. In addition, it is noticed that in the presence of additives, the porosity defect is minimal in addition to the tightly packed crystals. The fact that these clearly defined crystals are mostly round and are separated from one another by crystals with a rod-like shape also indicates that the electrodeposited zinc microstructure is of high quality and provides effective corrosion protection [36].

The result of EDS presented in Fig. 3 shows that the wt% of Zn electrodeposited on MS increased from 61.49% for the sample plated in the absence of additive to 93.84%, 90.37%, and 85.16% for samples plated in the presence of HME, EAE, and BE, respectively, implying that the presence of extracts as additives in the acid chloride bath significantly improves the Zn electrodeposition on MS [33].

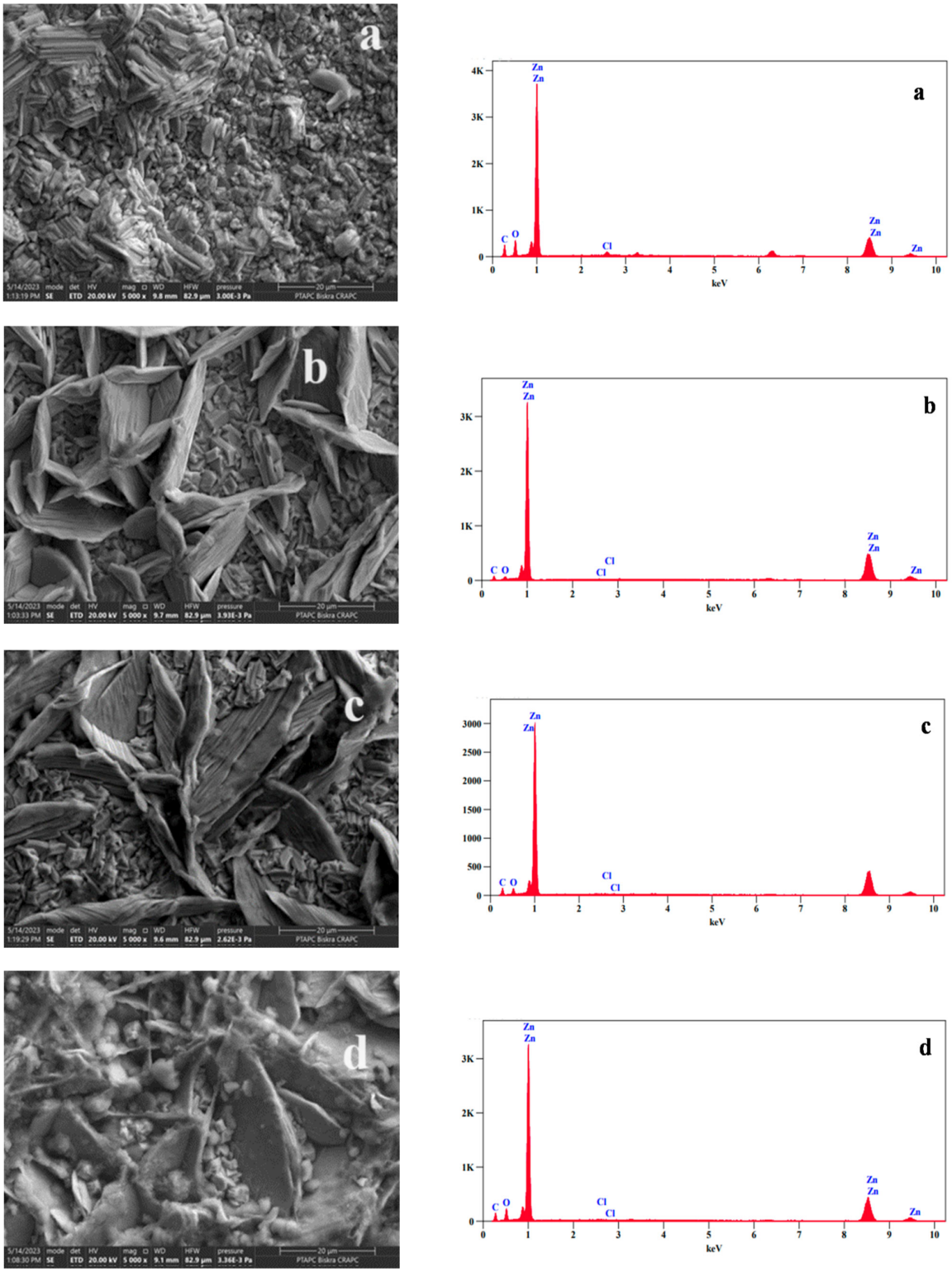

Fig. 3. SEM/EDS images of: MS surface-plated a) without additive; b) in the presence of 1.8 g/L of HME; c) 0.2 g/L of EAE; and d) 0.6 g/L of BE.

3.1.5 Profilometer analysis

Surface profilometry utilizes interference patterns generated by white light to enable exact and non-destructive measurements of surface profiles. Figure 4 shows the 3D surface morphologies of substrates with and without plant extracts, respectively. The color scale can be found on the right side of the surface profile, where the black-to-white color gradient represents the gradual increase in the height of the worn track profile. The black color indicates the lowest point of the valley, while the white color

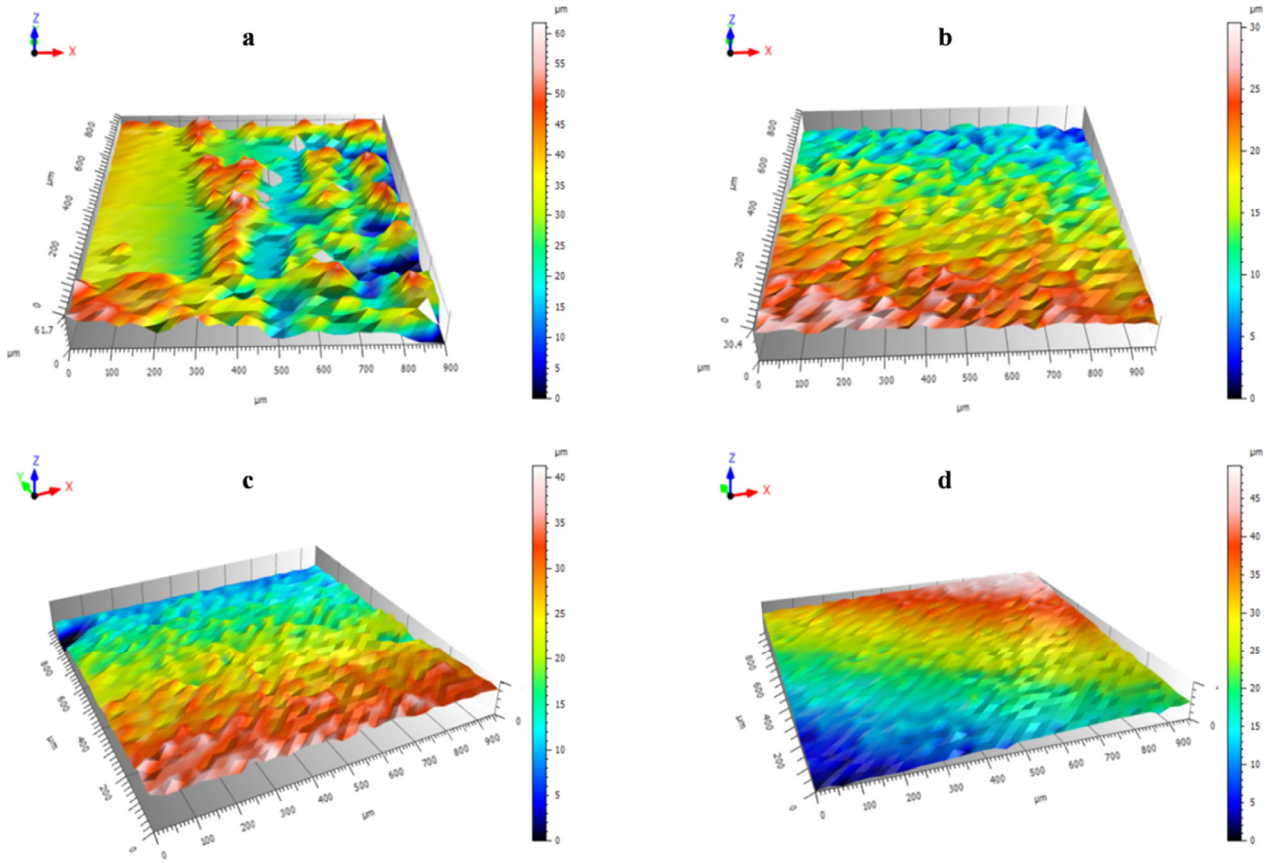

Fig. 4. Profilometer 3D images of plated MS a) without extract addition, b) in the presence of 1.8 g/L of HME, c) in the presence of 0.2 g/L of EAE, and d) in the presence of 0.6 g/L of BE.

indicates the highest point of the peak. It has been seen that the sample plated in the absence of plant extract exhibits more prominent surface features or irregularities, with more height variations than the sample plated in its presence, suggesting that it may have more significant surface roughness. This indicates that the plant extracts may play a role in smoothing or modifying the surface characteristics of the samples [36].

3.1.6 Area roughness parameters

According to ISO 25178 standards, Table 5 provides information related to the area roughness parameters. Table 4 shows that the presence of HME, EAE and BE results in a reduction in Sa, which stands for the arithmetical mean height of a surface (5.03 µm, 7.07 µm, and 8.77 µm respectively), compared to when it is plated without these substances (8.89 µm). This suggests that the surface becomes smoother when these substances are added. Furthermore, it has been observed that the use of extracts as an additive leads to a decrease in the root mean square height of a surface, represented by Sq. This indicates that the height deviations within the defined area

Table 4. Area roughness parameters

	ISO 25178			
	Without extract	HME	EAE	BE
Sq (µm)	11.30	5.98	8.27	10.60
Ssk	-0.28600	-0.02230	0.00519	-0.01400
Sku	3.00	2.19	2.09	2.33
Sp (µm	31.2	14.2	19.5	23.7
Sv (µm)	30.5	16.2	21.8	25.6
Sz (µm)	61.7	30.4	41.3	49.2
Sa (µm)	8.89	5.03	7.07	8.77

are decreasing, resulting in a smoother and uniform surface with lower roughness levels. The parameter Sz is determined by adding the highest peak height value and the largest pit depth value within the specified area, which means Sz=Sp+Sv (where Sp is the height of the highest peak and Sv is the absolute value of the height of the most considerable pit within the specified area). It is evident that there is a decrease in these parameters for samples plated in the presence of different plant extracts compared to the sample plated in their absence, indicating a

smoother surface. The Ssk parameters refer to the degree of bias of the roughness shape (asperity). When Ssk is less than 0, it means that the height distribution is skewed above the mean plane. A value of Ssk equal to 0 indicates that the height distribution (peaks and pits) is symmetrical around the mean plane. If Ssk is greater than 0, it signifies that the height distribution is skewed below the mean plane. Based on the values in Table 5, samples plated in the presence of plant extracts promote a more symmetrical distribution of surface roughness features, as indicated by skewness values close to 0. The Sku value, also known as Kurtosis, measures the sharpness of a roughness profile. A value less than 3 suggests that the height distribution is skewed above the mean plane. When Sku equals 3, it implies that the height distribution is standard, with both sharp and indented portions co-existing. However, if Sku exceeds 3, it indicates that the height distribution is spiked. Sku values from the table indicate that the samples plated in the presence of extracts have Sku values less than 3. This implies that adding extracts leads to a less sharp or spiked surface profile.

3.2. Corrosion Inhibitors

3.2.1 Potentiodynamic polarization measurements

Figure 5 shows the potentiodynamic polarization curves of the CS in 1M HCl solution without and with the addition of different concentrations of HME, MDE, EAE, and BE.

The analysis of Fig. 5 shows that adding different concentrations of HME, MDE, EAE, and BE to 1 M HCl changes both cathodic and anodic parts of the curves, which leads to lower current densities. That means that inhibitor adsorption on the SS could affect the cathodic and anodic reactions [19, 59].

It can be seen from Table 5 that the inhibitory efficiency increases with inhibitor concentration and reaches a maximum at 700 ppm (81.18%), 800 ppm (73.84%), 700 ppm (82.02%), and 700 ppm (78.11%), for HME, MDE, EAE, and BE, respectively. This increase is accompanied by a decrease in the current density, indicating that the addition of inhibitors reduces the anodic dissolution of steel and delays the evolution of hydrogen by simply adhering to the metal surface and blocking the active sites [61].

According to the literature [61-64], if the difference between the values of corrosion potential E_{corr}, in the presence and absence of an inhibitor, is greater than 85 mV/SCE, the inhibitor can be classified as cathodic or anodic. On the other hand, if this difference is less than 85 mV/SCE, the inhibitor is of mixed type. In the present work, the maximum potential value shift is in the order of 13.3 mV/SCE, suggesting that all the extracts tested are mixed-type inhibitors.

Table 5. Polarization parameters for corrosion of CS in 1M HCl in the absence and presence of various concentrations of plant extracts

Extract	C (ppm)	$-E_{corr}$ (mV/SCE)	i_{corr} (mA/cm²)	β_a (mV Dec^{-1})	$-\beta_c$ (mV Dec^{-1})	η_P (%)
	0	472.5	0.1430	75.9	101.0	/
HME	200	473.8	0.0422	54.9	137.6	70.48
	400	476.8	0.0360	57.1	123.0	74.82
	600	484.4	0.0329	66.7	129.1	76.99
	700	483.8	0.0269	82.6	125.6	81.18
MDE	200	476.8	0.0628	98.7	110.5	56.08
	400	474.8	0.0498	100.3	127.3	65.17
	600	472.4	0.0413	90.1	128.8	71.11
	800	485.3	0.0374	114.0	142.5	73.84
EAE	200	480.6	0.0505	106.5	122.6	64.68
	400	474.4	0.0376	53.2	108.0	73.70
	600	472.5	0.0332	96.9	139.1	76.78
	700	485.8	0.0257	93.8	110.4	82.02
BE	200	470.0	0.0413	60.2	160.6	71.11
	400	477.9	0.0411	56.4	145.3	71.25
	600	479.1	0.0375	104.8	137.3	73.77
	700	480.0	0.0313	98.2	135.8	78.11

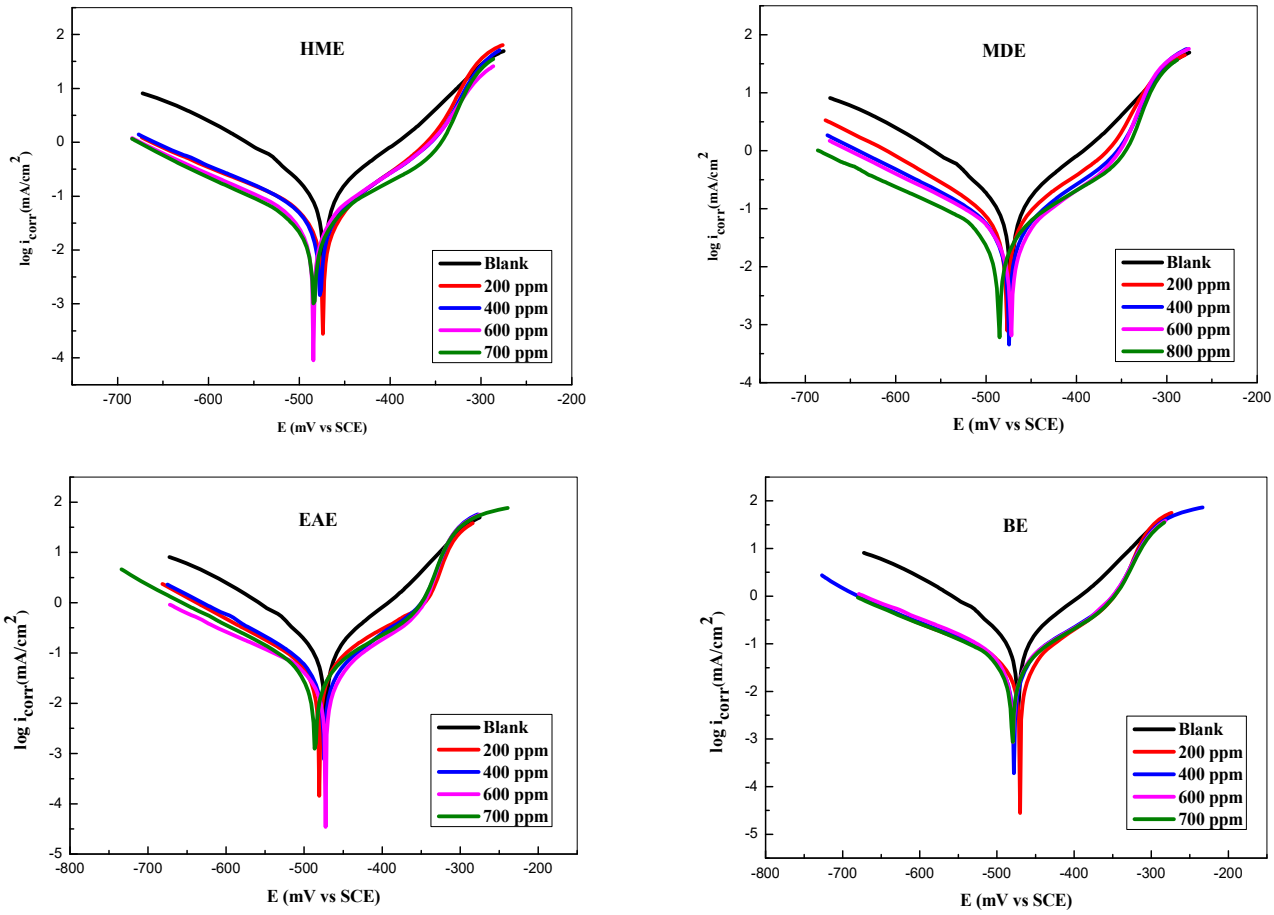

Fig. 5. Potentiodynamic polarization curves of CS in 1M HCl without and with various amounts of HME, MDE, EAE, and BE.

3.2.2 Electrochemical impedance spectroscopy (EIS)

Figure 6 shows the Nyquist diagrams for the CS in 1M HCl solution without and with the addition of different concentrations of HME, MDE, EAE, and BE.

As observed, these diagrams have a similar shape, which are semi-circles for all the tested specimens, indicating that the corrosion and its inhibition are controlled by the charge-transfer mechanism and that the reaction mechanism did not change after adding the inhibitor [64, 65]. Because the frequencies are spread out, and regarding the roughness and the non-uniformity of the electrode surface, these capacitive loops are not perfect [17, 65]. Furthermore, research reveals that the capacitive loop's diameter is more significant when the inhibitor is present compared to the blank solution, and gets bigger as the inhibitor's concentration rises, indicating an increase in charge transfer resistance [18, 66]. The Nyquist representation was fitted to the electrical equivalent circuit model (EEC) (Fig. 7). Both solution resistance (R_s) and charge transfer resistance (R_{ct}) are identified by the circuit.

It is worth noting that surface imperfections affect the double-layer capacitance (C_{dl}) value, which is simulated using a constant-phase element (CPE) [59]. The double-layer capacitance (C_{dl}) values are calculated using the given Eq. 9 [19, 38]:

$$C_{dl} = R_{ct}^{\frac{1-n}{n}} \times Q^{\frac{1}{n}} \quad (9)$$

where n is the deviation parameter of the CPE: 0≤n≤1, and Q is the magnitude of CPE identified with the capacity.

The electrochemical parameters and inhibitory efficacy η (%) obtained by electrochemical impedance spectroscopy using the equivalent circuitry for various concentrations of extracts are given in Table 6. From the results illustrated in Table 7, it is clear that an increase in the concentration of the inhibitor leads to a decrease in the values of the C_{dl}, while the reverse is the case for the charge transfer resistance, which increases. These results may be attributed to the thickening of the electric double layer, as well as a decrease in the dielectric constant

Table 6. Impedance parameters for corrosion of CS in 1M HCl in the absence and presence of various concentrations of plant extracts

Extract	C (ppm)	R_{ct} ($\Omega.cm^2$)	10^{-5} Q ($S^n\ \Omega^{-1}\ cm^{-2}$)	n	C_{dc} ($\mu Fcm^{-2)}$	η_R (%)
	0	119.2	77.8	0.572	132.30	/
HME	200	428.0	39.5	0.507	70.62	72.15
	400	492.8	24.8	0.605	63.57	75.81
	600	535.8	18.4	0.623	45.68	77.75
	700	640.5	17.9	0.609	45.00	81.39
MDE	200	304.6	31.3	0.634	80.69	60.86
	400	468.6	23.7	0.656	75.33	74.56
	600	576.7	21.9	0.618	61.59	79.33
	800	660.7	19.4	0.547	35.66	81.96
EAE	200	299.0	48.8	0.536	92.53	60.13
	400	477.5	27.0	0.641	86.36	75.03
	600	510.5	18.7	0.653	54.27	76.65
	700	554.7	18.4	0.638	51.05	78.51
BE	200	440.3	38.3	0.526	77.62	72.93
	400	459.9	34.3	0.501	54.82	74.08
	600	544.3	21.5	0.551	37.59	78.10
	700	597.2	16.8	0.587	33.69	80.04

Table 7. Corrosion parameters from weight loss measurements of CS in a 1M HCl solution containing various concentrations of HME, MDE, EAE, and BE at different temperatures

	C (ppm)	Temperature											
		293 K			303 K			313 K			323 K		
		CR (mg $cm^{-2}\ h^{-1}$)	Θ	η_w (%)	CR (mg $cm^{-2}\ h^{-1}$)	Θ	η_w (%)	CR (mg $cm^{-2}\ h^{-1}$)	Θ	η_w (%)	CR (mg $cm^{-2}\ h^{-1}$)	Θ	η_w (%)
	blank	0.1376	-	-	0.2049	-	-	0.2530	-	-	0.3793	-	-
HME	200	0.0334	0.7573	75.73	0.0866	0.5774	57.74	0.1210	0.5217	52.17	0.2637	0.3048	30.48
	400	0.0297	0.7842	78.42	0.0712	0.6525	65.25	0.1014	0.5992	59.92	0.2468	0.3493	34.93
	600	0.0286	0.7922	79.22	0.0659	0.6784	67.84	0.0946	0.6261	62.61	0.2134	0.4374	43.74
	700	0.0213	0.8452	84.52	0.0591	0.7116	71.16	0.0752	0.7028	70.28	0.1941	0.4883	48.83
MDE	200	0.0589	0.5719	57.19	0.1090	0.4680	46.80	0.1479	0.4154	41.54	0.2334	0.3846	38.46
	400	0.0524	0.6191	61.91	0.0923	0.5495	54.95	0.1159	0.5418	54.18	0.1979	0.4782	47.82
	600	0.0409	0.7027	70.27	0.0747	0.6354	63.54	0.1017	0.5980	59.80	0.1713	0.5483	54.83
	700	0.0379	0.7245	72.45	0.0654	0.6808	68.08	0.0929	0.6328	63.28	0.1496	0.6055	60.55
	800	0.0349	0.7463	74.63	0.0604	0.7052	70.52	0.0814	0.6782	67.82	0.1432	0.6224	62.24
EAE	200	0.0596	0.5669	56.69	0.0990	0.5168	51.68	0.1349	0.4668	46.68	0.2157	0.4313	43.13
	400	0.0393	0.7143	71.43	0.0832	0.5939	59.39	0.1170	0.5375	53.75	0.1931	0.4909	49.09
	600	0.0327	0.7623	76.23	0.0704	0.6564	65.64	0.1001	0.6043	60.43	0.1653	0.5642	56.42
	700	0.0223	0.8379	83.79	0.0578	0.7179	71.79	0.0839	0.6684	66.84	0.1421	0.6254	62.54
BE	200	0.0487	0.6461	64.61	0.0901	0.5603	56.03	0.1328	0.4751	47.51	0.2151	0.4329	43.29
	400	0.0331	0.7594	75.94	0.0698	0.6593	65.93	0.1174	0.5359	53.59	0.1994	0.4743	47.43
	600	0.0318	0.7689	76.89	0.0679	0.6686	66.86	0.1134	0.5518	55.18	0.1783	0.5299	52.99
	700	0.0302	0.7805	78.05	0.0603	0.7057	70.57	0.1026	0.5945	59.45	0.1596	0.5792	57.92

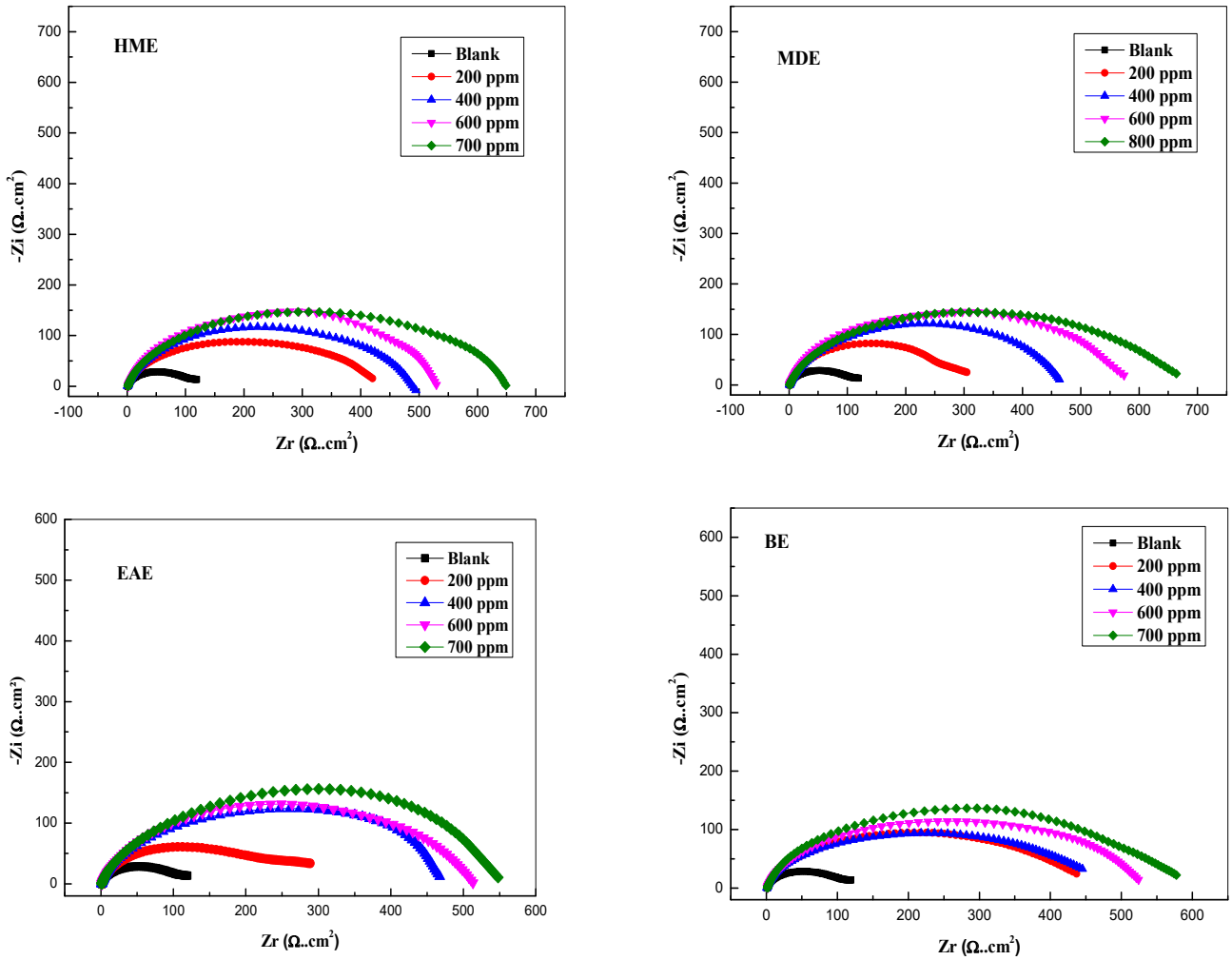

Fig. 6. Nyquist diagrams for the CS in 1M HCl solution in the absence and presence of HME, MDE, EAE, and BE at various concentrations.

and an increase in surface coverage, respectively [67]. The highest levels of inhibition efficiency were obtained at concentrations of 700 ppm (81.39%), 800 ppm (81.96%), 700 ppm (78.51%), and 700 ppm (80.04%), respectively, for HME, MDE, EAE, and BE. These results are comparable to other green corrosion inhibitors, such as extracts from *Aerva lanata* (88%) [68], *Syzygium cumini* (83.5%) [69], and *Datura stramonium* (94.2%) [70].

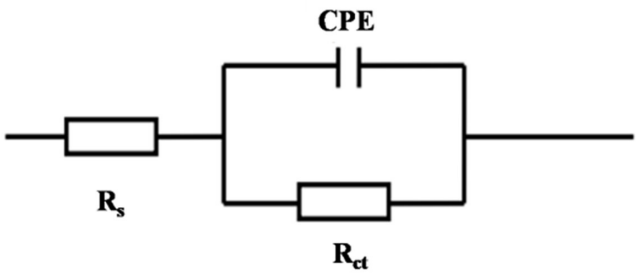

Fig. 7. Equivalent circuit used to fit the capacitive loop.

3.2.3 Weight loss studies

Table 7 provides the summarized inhibition efficiency η_w (%) and corrosion rate CR values acquired using the weight loss method at various inhibitor concentrations and temperatures. Table 7, Fig. 8 shows that increasing the concentration of the inhibitor leads to a drop in CR and an increase in η_w (%). The maximum corrosion inhibition efficiency (84.52%) was found for HME at 700 ppm, while it reached 74.63%, 83.79%, and 78.05% for MDE, EAE, and BE at 800 ppm, 700 ppm, and 700 ppm, respectively. The effectiveness of stopping corrosion, which goes up as the concentration of inhibitors increases, is attributed to the adsorption of inhibitor molecules on the metallic surface, which slows down the dissolution process [71]. However, the increase in CR with increasing temperature is typically attributed to the higher dissolution of the metal and may also be attributed to the rise in the solubility of the metal's protective films [72-74].

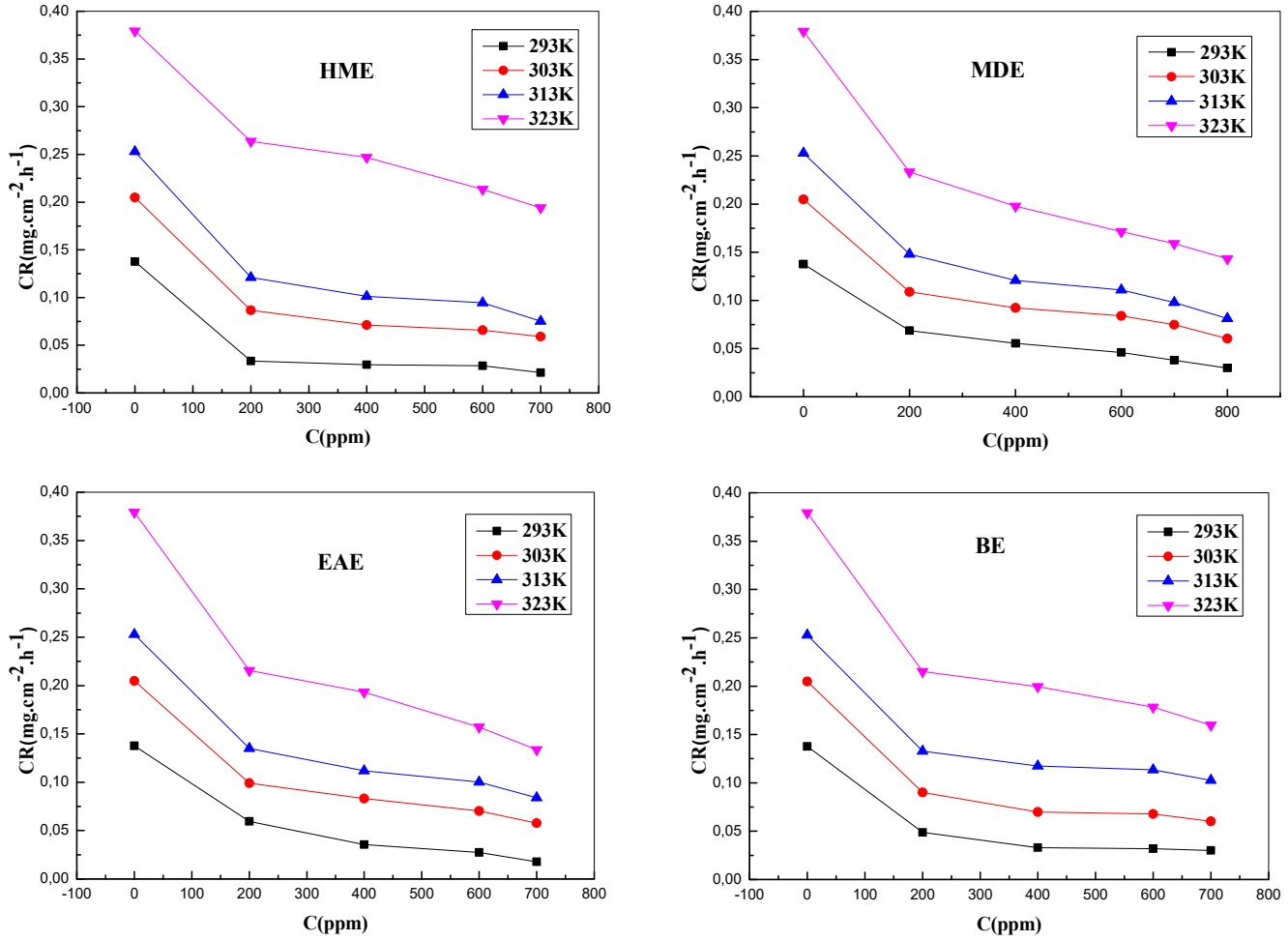

Fig. 8. Variation of the corrosion rate as a function of various concentrations of HME, MDE, EAE, and BE in a 1M HCl solution at different temperatures.

3.2.4 Adsorption isotherm and thermodynamic parameters

It is widely understood that corrosion is inhibited by the adsorption of the inhibitor's molecules [756]. After investigating the Langmuir, Temkin, and Freundlich isotherms to see which one fits the current study the best, and it was found that Langmuir provided the best graphical fit (Eq. 10). It is important to underline that the fitted model isotherm assumes monolayer adsorption of the inhibitor on the metal surface without interactions between the adsorbed species [76].

$$\frac{C}{\theta} = \frac{1}{K_{ads}} + C \qquad (10)$$

where θ is the surface coverage, C is the inhibitor concentration and K_{ads} is the equilibrium constant of the adsorption process.

The plot of the Langmuir isotherm (Fig. 9) allows the determination of the equilibrium constant of the adsorption process (K_{ads}) from the intercept.

Based on the relationship shown in the Eq. 11, the standard Gibbs free energy of the adsorption process can be determined [77]:

$$\Delta G^{o}_{ads} = -RT\ln(C_{H_2O} \cdot K_{ads}) \qquad (11)$$

where R is the gas constant, T is the absolute temperature (K), and $C(H_2O)$ is the concentration of water expressed inmg.l^{-1} with an approximate value of 10^6 [78].

The standard adsorption enthalpy ($\Delta H°_{ads}$) can be calculated using the Van't Hoff Eq. 12, as shown below [73]

$$\frac{d\ln K_{ads}}{dT} = \frac{\Delta H^{o}_{ads}}{RT^2} \qquad (12)$$

Equation 12 can be rewritten as follows [79]:

$$\ln K_{ads} = -\frac{\Delta H^{o}_{ads}}{RT} + I \qquad (13)$$

where I is a constant of integration.

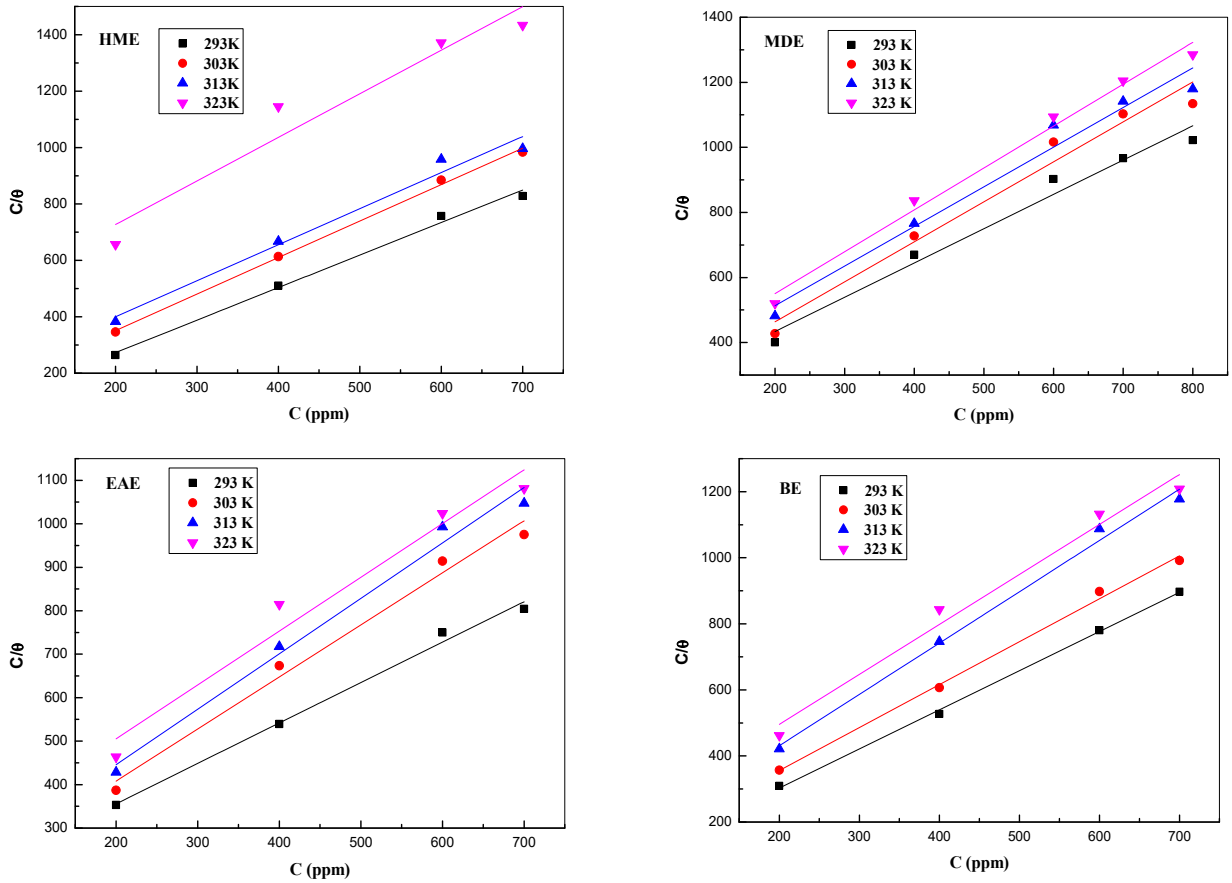

Fig. 9. The Langmuir adsorption isotherm of HME, MDE, EAE, and BE on CS in a solution of 1M HCl at different temperatures.

The variation of $\ln K_{ads}$ as a function of the inverse of the temperature (Fig. 10) is a straight line with a slope $-\frac{\Delta H^{o}_{ads}}{R}$ from which we can derive the value of (ΔH°_{ads}).

The values of standard adsorption entropy ΔS°_{ads} are calculated from the Gibbs Helmholtz equation [42].

$$\Delta S^{o}_{ads} = \frac{\Delta H^{o}_{ads} - \Delta G^{o}_{ads}}{T} \qquad (14)$$

The standard thermodynamic parameters of HME, DME, EAE, and BE adsorption in 1M HCl solution are summarized in Table 8 and Fig. 10.

Table 8 shows that the K_{ads} values for all tested extracts decrease as the temperature rises, which may be a sign that the adsorbed inhibitors from the SS are desorbing [19]. Additionally, Table 8 reveals that all ΔG°_{ads} values were negative, which demonstrates the spontaneity of the adsorption process on the surface of CS [80]. Generally, the values of ΔG°_{ads} neighboring -20 KJ.mol^{-1} or less negative are linked to electrostatic interactions between charged molecules and charged metals [74].

In this study, the calculated values of ΔG°_{ads} varied between -24.54 KJ.mol^{-1} and -20.89 KJ.mol^{-1}, which suggests that the adsorption of all extracts on the metallic surface is of the physical type at different temperatures [81]. The values of the thermodynamic adsorption parameters can provide information on the inhibition of corrosion. An endothermic adsorption process (ΔH°_{ads}>0) can be attributed to chemisorption, whereas an exothermic adsorption

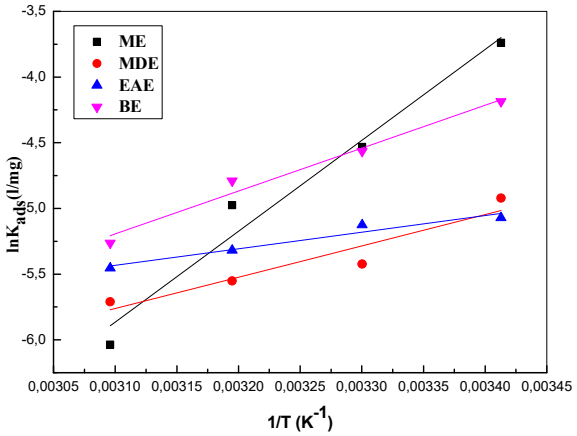

Fig. 10. Variation of $\ln K_{ads}$ as a function of the inverse of the temperature.

Table 8. Standard thermodynamic parameters

Extract	Temperature (K)	r^2	K_{ads}(l.mg^{-1})	$\Delta G°_{ads}$(KJ.mol^{-1})	$\Delta H°_{ads}$(KJ.mol^{-1})	$\Delta S°_{ads}$(J.mol^{-1}K^{-1})
HME	293	0.99155	0.02378	-24.54	-57.55	-112.66
	303	0.99704	0.01076	-23.38		-112.77
	313	0.97254	0.00691	-23.01		-110.35
	323	0.91165	0.00239	-20.89		-113.49
MDE	293	0.99178	0.00729	-21.66	-19.81	6.31
	303	0.98581	0.00441	-21.14		4.38
	313	0.99055	0.00388	-21.50		5.39
	323	0.98304	0.00331	-21.77		6.06
EAE	293	0.98602	0.00627	-21.30	-10.47	36.96
	303	0.98004	0.00594	-21.89		37.68
	313	0.97089	0.00490	-22.11		37.18
	323	0.96200	0.00428	-22.45		37.08
BE	293	0.99833	0.01520	-23.46	-27.12	-12.49
	303	0.99554	0.01042	-23.31		-12.57
	313	0.99053	0.00831	-23.49		-11.59
	323	0.97358	0.00518	-22.97		-12.84

process ($\Delta H°_{ads}$<0) can involve physisorption and/or chemisorption [81, 82]. In our case, the $\Delta H°_{ads}$ values are -57.55 KJ.mol^{-1}, -19.81 KJ.mol^{-1}, -10.47 KJ.mol^{-1}, end -27.12 KJ.mol^{-1} for HME, MDE, EAE, and BE, respectively, indicating an exothermic adsorption process. Although these negative enthalpy values suggest a complex interaction that could involve chemisorption or mixed mechanisms, the observed decrease in corrosion rate with increasing temperature supports the dominance of physical adsorption. This behavior aligns with typical physical adsorption processes, where adsorption decreases as temperature rises, confirming the previous findings of physical adsorption for all extracts on SS [78]. The entropy of the HME and BE has a negative sign, indicating that it goes down during the adsorption process, which can be explained as the degree of disorder in the extract's molecules is significant before adsorption on the SS, but they become less disorganized after their adsorption non the steel surface [59, 78]. The MDE and EAE, on the other hand, have a positive adsorption entropy sign. This is because inhibitors stick to the SS through a process of quasi-substitution between the inhibitor molecules and water molecules on the electrode's surface. It can also be attributed to an increase in the disorder that occurs during the formation of reactants at the metal/solution interface, which is the driving force for the adsorption of inhibitor compounds to the metal surface [83, 84]. The differing entropy behaviors of HME/BE and MDE/EAE during adsorption can be attributed to their distinct molecular interactions and surface alignment. The entropy of HME and BE exhibits a negative sign, indicating reduced disorder during adsorption. This arises from their strong hydrogen bonds, which promote molecular organization before adsorption. Upon binding to the steel surface, these molecules align uniformly, further decreasing disorder. In contrast, MDE and EAE show positive entropy values, reflecting increased disorder. This is attributed to a quasi-substitution process: inhibitor molecules displace water molecules on the electrode surface, creating new configurations at the metal/solution interface and introducing disorder. For HME and BE, the pre-existing molecular order (due to hydrogen bonds) contribute to a more structured arrangement before adsorption, and upon adsorption, the molecules become even more organized as they align with the surface, reducing overall disorder.

3.2.5 Activation parameters of the corrosion process

The activation energy is calculated using Arrhenius Eq. 15 [85].

$$\ln CR = -\frac{E_a}{RT} + \ln D \quad (15)$$

where E_a is the apparent activation energy, and D is the Arrhenius pre-exponential factor.

The variation of the logarithm of the corrosion rate lnCR as a function of the inverse of the temperature of the 1M HCl solution without and with extract is shown in Fig. 11. The slopes of the straight lines $-\frac{E_a}{R}$ for varied inhibitor doses are used to calculate the apparent activation energies. In this research, the activation energies that were found when HME, MDE, EAE, and BE were present at different concentrations ranging from 32.79 KJ mol^{-1} to 54.06 KJ mol^{-1} were higher than the value (25.57 KJ mol^{-1}) obtained in the absence of an inhibitor. Many authors [86-88] attribute this rise in activation energy because the inhibitors physically adsorb on the SS and their adsorption decreases as the temperature rises due to the increased inhibitor desorption at higher temperatures. An alternative formula for Arrhenius allows the determination of the activation enthalpy $\Delta H°_a$ and the activation entropy in the corrosion process of steel in the acid medium. These parameters are provided by Eq. 16 [89]:

$$CR = \frac{RT}{N_a h} \exp\frac{\Delta S^o_a}{R} \exp\left(-\frac{\Delta H^o_a}{RT}\right) \quad (16)$$

where h is the Planck constant, and N_a is the Avogadro number.

The variation of the $\ln\frac{CR}{T}$ as a function of the inverse of the temperature $\frac{1}{T}$ is a straight line (Fig. 12) with a slope of $-\frac{\Delta H^o a}{R}$ and ordinate at the origin equals $\ln\frac{R}{N_a h} + \frac{\Delta S^o a}{R}$.

The positive signs of the activation enthalpies $\Delta H°_a$ represents the endothermic nature of the CS dissolution process [90]. Activation enthalpies and activation entropies are listed in Table 9. Concerning the entropy of activation $\Delta S°_a$, the positive values obtained for the 1M HCl solutions containing different concentrations of HME are due to the water molecules being replaced during the adsorption of inhibitors on the metallic surface [91]. On the other hand, the negative values of the MDE, EAE, and BE showed that the active rate-determining step represents an association rather than a dissociation, demonstrating that a reduction in the disorder takes place [19].

3.2.6. Scanning electron microscopy with energy dispersive spectroscopy (SEM/EDS) for corrosion inhibition

SEM and EDS analyses were used to examine the surface morphology of CS specimens and identify the elements present in corroded and inhib-

Table 9. Activation parameters for CS in 1M HCl with different concentrations of HME, DME, EAE, and BE and in their absence

Extract	C (ppm)	E_a (KJ mol^{-1})	ΔH_a (KJ mol^{-1})	$10^{-1}\ \Delta S_a$ (J mol^{-1} K^{-1})
Blank	0	25.57	23.02	-18.26
HME	200	51.47	48.91	-27.19
	400	52.73	50.17	27.49
	600	50.27	47.71	26.62
	700	54.06	51.51	27.71
MDE	200	34.96	32.40	-15.73
	400	33.15	30.60	-16.46
	600	36.25	33.70	-15.60
	700	35.18	32.63	-16.04
	800	35.64	33.08	-15.96
EAE	200	32.79	30.24	-16.49
	400	40.36	37.81	-14.20
	600	41.13	38.57	-14.09
	700	46.84	44.28	-12.42
BE	200	38.16	35.60	-14.81
	400	46.56	44.01	-12.25
	600	44.85	42.30	-12.85
	700	43.58	41.02	-13.34

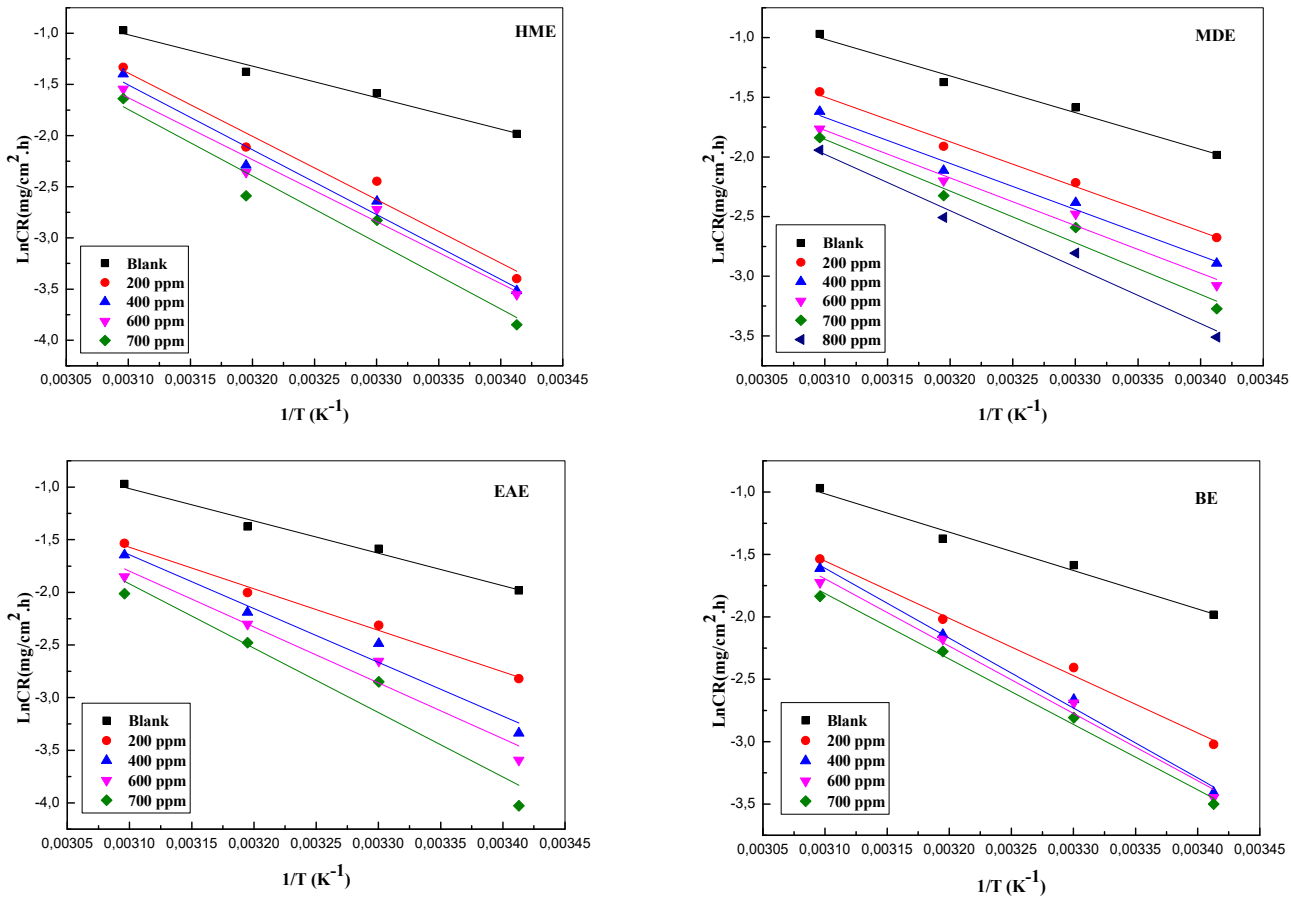

Fig. 11. Arrhenius plots of LnCR versus $\frac{1}{T}$ for CS corrosion in 1M HCl of HME, MDE, EAE, and BE.

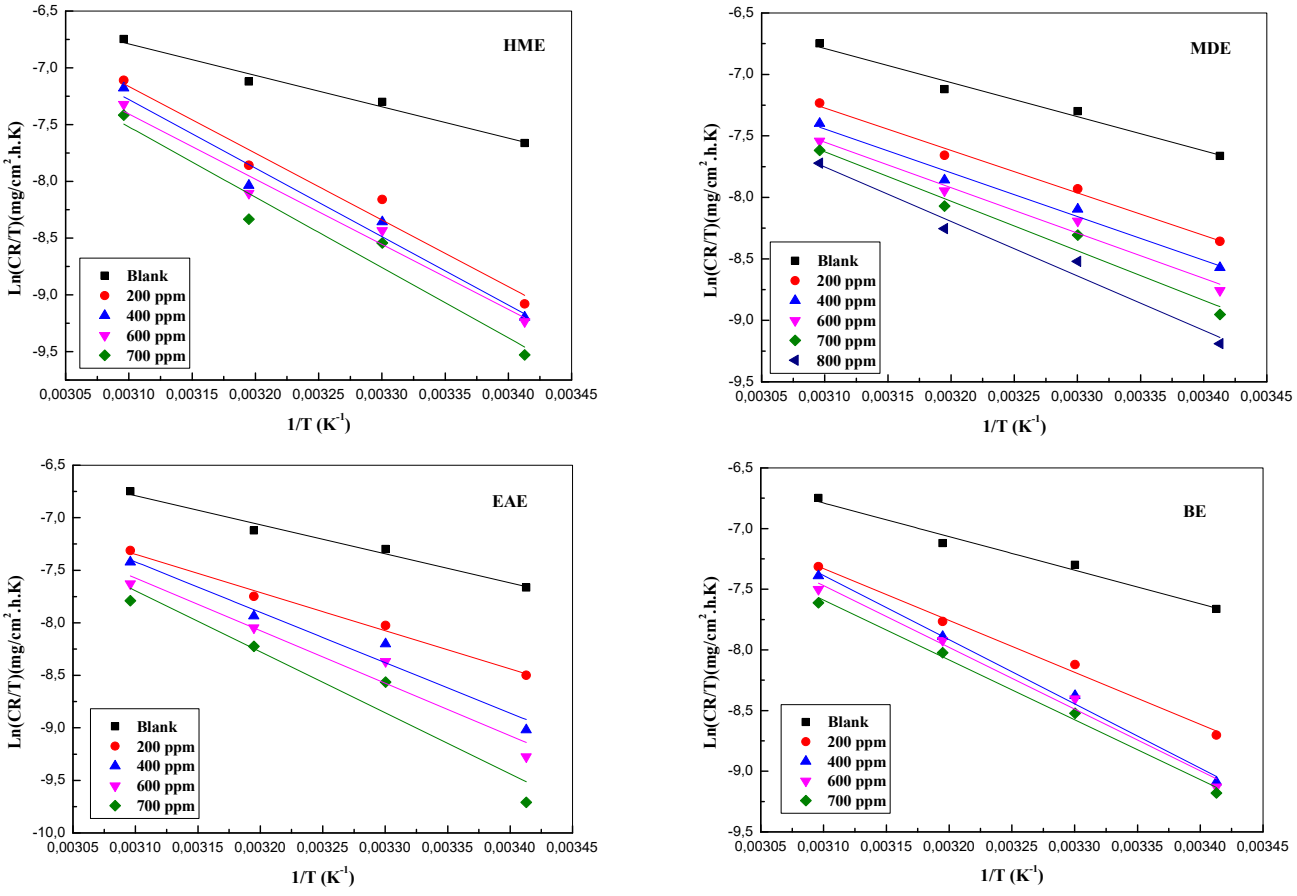

Fig. 12. Arrhenius plots of $\ln\frac{CR}{T}$ versus $\frac{1}{T}$ for CS corrosion in 1 M HCl of HME, MDE, EAE, and BE.

ited metal surfaces. Figure 13 and Table 10 show the resulting morphologies, spectra, and chemical composition before and after 2 hours of immersion in uninhibited and inhibited HCl solutions, respectively. Figure 13 clearly illustrates that by subjecting the specimen to 1 M HCl (blank), the surface morphology was severely damaged due to the acid corrosion attack. The appearance of the O signal in the EDS spectrum serves as evidence for the formation of iron oxides, which confirms the extent of the damage caused by acid corrosion [60, 92]. However, after being submerged in an acidic solution containing 700, 800, 700, and 700 ppm of HME, MDE, EAE, and BE, respectively, the specimen's surface was smoother with few cracks and pits; this can be explained by the formation of a barrier film due to the inhibitor molecules adsorption [93].

The corresponding EDS spectra and element percentages (Table 10) revealed that the O peak was absent in the EDS spectrum for all tested extracts, indicating that the inhibitors were highly effective in slowing corrosion [92].

The observed surface morphology changes correlate directly with electrochemical performance. Uninhibited HCl exposure produced severely damaged, oxide-rich surfaces (evidenced by elevated O signals in EDS), which aligned with low charge transfer resistance (R_{ct}) and high corrosion current (i_{corr}) in EIS and potentiodynamic polarization. In contrast, inhibited surfaces exhibited smoother morphologies with fewer defects (reduced O/Cl in EDS), correlating with enhanced electrochemical behavior (higher R_{ct}), lower i_{corr}) and high corrosion inhibition efficiency. The smoother surfaces resulted from inhibitor adsorption, which reduced active corrosion sites and defects, thereby minimizing charge transfer and corrosion propagation.

3.2.7 Mechanism of inhibition

As mentioned earlier, corrosion inhibition occurs primarily through the adsorption of inhibitors onto the metal surface [75]. This process depends on the inhibitor's nature, charge, and chemical structure, as well as the chemical composition of the solution and the metallic surface's charge [90, 94]. The charge of the metal surface is determined by the E_{corr}-E_q=0 value, which for steel (Iron) is around -530 mV/SCE in a 1M HCl solution [42, 95]. In this investigation, E_{corr} was measured at approximately -472 mV/SCE. As the obtained value of E_{corr}-E_q=0>0, it can be inferred that the surface of the steel is positively charged [77, 95].

Regarding the inhibitor, the complex chemical composition of the plants explains the difficulty of attributing the inhibitory effect of absorption to any particular component, since some of these constituents include tannins, flavonoids, alkaloids, etc. In an acid medium, the inhibitory effect of plant extracts is attributed by several authors to the protonation of the majority of the organic molecules of these extracts, which makes them positively charged [19, 42, 75]. And since the metallic surface is also positively charged, repulsion forces between the protonated molecules and the metallic surface may occur. In this case, the Cl- anions of the hydrochloric solution will be the first to be adsorbed on the metal surface. This first adsorption makes the surface negative, and then the adsorption of the inhibiting molecules is induced by the electrostatic attraction between the negative charges of the surface and the positive charges of each extract, resulting in a reduction in the dissolution of the steel [71, 96].

This paper has been presented as an early online preprint version, which was not peer-reviewed [97].

Table 10. Chemical composition of CS immersed in 1 M HCl solution without and with the addition of 700 ppm HME, 800 ppm MDE, 700 ppm EAE, and 700 ppm BE

		Fe	C	O	Cl
HCl 1M	wt%	94.37	2.20	3.37	0.06
	Atom %	81.05	8.77	10.10	0.08
HME	wt%	98.35	1.65	0.00	0.00
	Atom %	92.75	7.25	0.00	0.00
MDE	wt%	99.42	0.58	0.00	0.00
	Atom %	97.38	2.62	0.00	0.00
EAE	wt%	99.31	0.69	0.00	0.00
	Atom %	96.89	3.11	0.00	0.00
BE	wt%	98.91	1.05	0.00	0.04
	Atom %	95.23	4.71	0.00	0.06

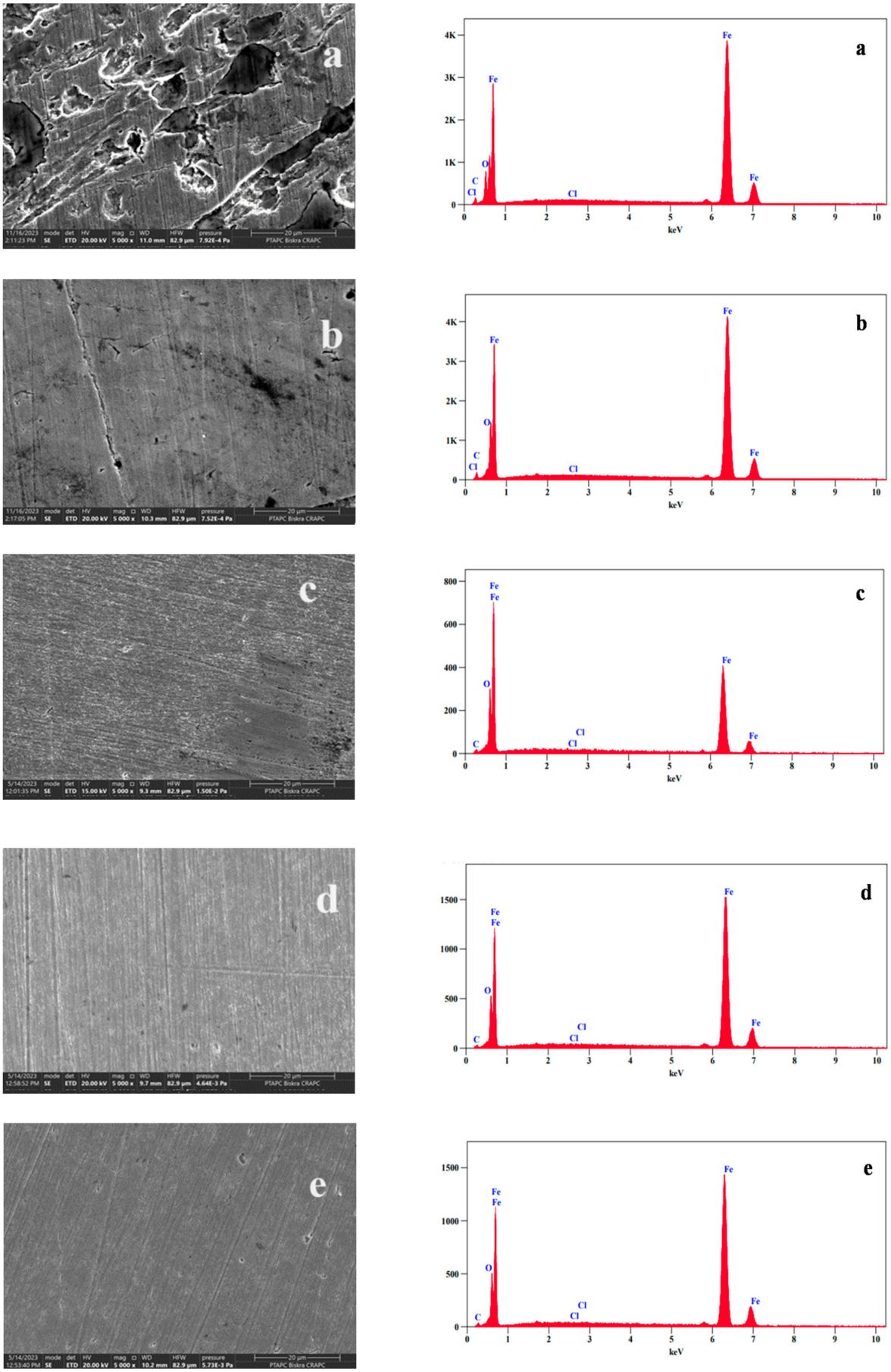

Fig. 13. SEM/EDS images of CS immersed in: a) 1 M HCl solution; and in 1 M HCl containing: b) 700 ppm HME, c) 800 ppm MDE, d) 700 ppm EAE, and e) 700 ppm BE.

4. Conclusions

The performance of *Centaurea napifolia* extracts working as additives in a zinc-electroplating bath and as corrosion inhibitors in an acidic medium was studied and discussed, leading to the following conclusions. All plant extracts exhibited good corrosion inhibition efficiency, particularly in an acidic environment via physical adsorption obeying the Langmuir model, and they are mixed-type inhibitors. *Centaurea napifolia* extracts effectively prevent mild steel corrosion in acidic environments, as evidenced by consistent results from weight loss and electrochemical measurements. The inhibition efficiencies of the extracts HME, MDE, EAE, and BE were calculated as medium to high, averaging 82.36%, 76.81%, 81.44%, and 79%, respectively, across the three techniques used: weight loss, EIS, and potentiodynamic polarization. This comparative analysis highlights that HME exhibited the highest efficiency, closely followed by EAE, while BE and MDE showed slightly lower efficiencies. The SEM and EDS spectra, which demonstrate that the inhibition occurred after the adsorption mechanism, support these findings. Plant extracts, excluding MDE, significantly impacted the morphology of the electroplated coating, potentially improving corrosion resistance properties and leading to brighter, smoother, and more adherent electroplated coatings. The morphology and the roughness of coatings evaluated using SEM/EDS and the profilometer indicate a uniform and smooth coating for the samples plated in the presence of HME, EAE, and BE. However, scalability and cost-effectiveness are key challenges for widespread adoption. Assessing long-term performance and durability across various environmental conditions is also crucial.

Future research should explore optimizing conditions for the industrial implementation of these natural additives. Additionally, investigating other plant extracts or synergistic combinations could further enhance corrosion inhibition properties while maintaining eco-friendliness.

Acknowledgment

The authors are grateful to Echahid Cheikh Larbi Tebessi University for providing facilities realize this work. We also appreciate the research facilities provided by the ANABIB gas pipes unit in Tebessa (Algeria) and the Fat Factory ENAP Souk-Ahras (Algeria) laboratory.

References

[1]. T. Clarkson, Health effects of metals: a role for evolution? *Environ. Health Perspect*. 103 (1995) 9-12. DOI: 10.1289/ehp.95103s19

[2]. E. Elqars, M. Guennoun, N. Sqalli Houssini, A. Thoume, I. Mechnou, A. Essadki, T. Nbigui, The adsorption performance of chicken excrement extract as corrosion inhibition of carbon steel in a 1 M HCl medium. *J. Bio-Tribo-Corros.* 7 (2021) 1-12. DOI: 10.1007/s40735-021-00520-9

[3]. S.H. Alrefaee, K.Y. Rhee, C. Verma, M.A. Quraishi, E.E. Ebenso, Challenges and advantages of using plant extract as inhibitors in modern corrosion inhibition systems: Recent advancements. *J. Mol. Liq.* 321 (2021) 114666. DOI: 10.1016/j.molliq.2020.114666

[4]. A. Thomas, M. Prajila, K.M. Shainy, A. Joseph, A green approach to corrosion inhibition of mild steel in hydrochloric acid using fruit rind extract of *Garcinia indica* (Binda). *J. Mol. Liq.* 312 (2020) 113369. DOI: 10.1016/j.molliq.2020.113369

[5]. N. Chaubey, Savita, A. Qurashi, D.S. Chauhan, M.A. Quraishi, Frontiers and advances in green and sustainable inhibitors for corrosion applications: A critical review. *J. Mol. Liq.* 321 (2021) 114385. DOI: 10.1016/j.molliq.2020.114385

[6]. A. Bouoidina, E. Ech-Chihbi, F. El-Hajjaji, B. El Ibrahimi, S. Kaya, M. Taleb, Anisole derivatives as sustainable-green inhibitors for mild steel corrosion in 1 M HCl: DFT and molecular dynamic simulations approach, *J. Mol. Liq.* 324 (2021) 115088. DOI: 10.1016/j.molliq.2020.115088

[7]. B.R. Holla, R. Mahesh, H.R. Manjunath, V. Raghu Anjanapura, Plant extracts as green corrosion inhibitors for different kinds of steel: A review. *Heliyon* 10 (2024) e33748. DOI: 10.1016/j.heliyon.2024.e33748

[8]. M. Benahmed, I. Selatnia, N. Djeddi, S. Akkal, H. Laouer, Adsorption and corrosion inhibition properties of butanolic extract of *Elaeoselinum thapsioides* and its synergistic effect with *Reutera lutea* (Desf.) Maires (Apiaceae) on A283 carbon steel in hydrochloric acid solution. *Chem. Afr*. 3 (2020) 251-261. DOI: 10.1007/s42250-019-00093-8

[9]. G. Ong, R. Kasi, R. Subramaniam, A review on plant extracts as natural additives in coating applications. *Prog. Org. Coat.* 151 (2021) 106091. DOI: 10.1016/j.porgcoat.2020.106091

[10]. J. Ajayi-Majebi, O.P. Abioye, O.S.I. Fayomi, A.O. Inegbenebor, Review of electrodeposition perspectives towards anticorrosion mitigation of mild steel. *IOP Conf. Ser.: Mater. Sci. Eng.* 1107 (2021) 012082. DOI: 10.1088/1757-899X/1107/1/012082

[11]. A. Mahapatro, S.K. Suggu, Modeling and simulation of electrodeposition: effect of electrolyte current density and conductivity on electroplating thickness. *Adv. Mater. Sci.* 3 (2018). DOI: 10.15761/AMS.1000143

[12]. O.S.I. Fayomi, D. Olusanyan, C.A. Loto, N.E. Udoye, Insight on the Electrodeposition Technology and Parameter for Corrosion Control of Structural Steel. *IOP Conf. Ser. Mater. Sci. Eng.* 1036 (2021) 012056. DOI: 10.1088/1757-899X/1036/1/012056

[13]. I.M. Omar, K.M. Emran, M. Aziz, A.M. Al-Fakih, A novel viewpoint of an imidazole derivative ionic liquid as an additive for cobalt and nickel electrodeposition. *RSC Adv.* 10 (2020) 32113-32126. DOI: 10.1039/D0RA06510B

[14]. M. Srivastava, V.E. Selvi, V.W. Grips, K.S. Rajam, Corrosion resistance and microstructure of electrodeposited nickel–cobalt alloy coatings. *Surf. Coat. Technol.* 201 (2006) 3051-3060. DOI: 10.1016/j.surfcoat.2006.06.017

[15]. A. Zaabar, E. Rocca, D. Veys-Renaux, R. Aitout, H. Hammache, L. Makhloufi, K. Belhamel, Influence of nettle extract on zinc electrodeposition in an acidic bath: Electrochemical effect and coating morphology, *Hydrometallurgy* 191 (2020) 105186. DOI: 10.1016/j.hydromet.2019.105186

[16]. Y. Yang, S. Liu, X. Yu, C. Huang, S. Chen, G. Chen, Q.H. Wu, Effect of additive on zinc electrodeposition in acidic bath, *Surf. Eng*. 31 (2015) 446-451. DOI: 10.1179/1743294415Y.0000000006

[17]. S. Shivakumara, U. Manohar, Y. Arthoba Naik, T.V. Venkatesha, Effect of condensation product on electrodeposition of zinc on mild steel, *Bull. Mater. Sci.* 30 (2007) 463-468. DOI: 10.1007/s12034-007-0073-y

[18]. K. Hanini, M. Benahmed, S. Boudiba, I. Selatnia, S. Akkal, H. Laouer, Experimental and Theoretical Studies of *Taxus baccata* Alkaloid Extract as Eco-Friendly Anticorrosion for Carbon Steel in Acidic Solution. *Prot. Met. Phys. Chem. Surf.* 57 (2021) 222-233. DOI: 10.1134/S2070205120060118

[19]. K. Hanini, M. Benahmed, S. Boudiba, I. Selatnia, H. Laouer, S. Akkal, Influence of different polyphenol extracts of *Taxus baccata* on the corrosion process and their effect as additives in electrodeposition. *Sustainable Chemistry and Pharmacy* 14 (2019) 100189. DOI: 10.1016/j.scp.2019.100189

[20]. S.A. Hussein, A.A. Khadom, Okra leaves extract as green corrosion inhibitor for steel in sulfuric acid: Gravimetric, electrochemical, and surface morphological investigations. *Results Chem.* 8 (2024) 101566. DOI: 10.1016/j.rechem.2024.101566

[21]. I. Selatnia, A. Sid, M. Benahmed, O. Dammene Debbih, T. Ozturk, N. Gherraf, Synthesis and characterization of a bis-pyrazoline derivative as corrosion inhibitor for A283 carbon steel in 1M HCl: electrochemical, surface, DFT and MD simulation studies. *Prot. Met. Phys. Chem. Surf*. 54 (2018) 1182-1193. DOI: 10.1134/S2070205118060229

[22]. A. Miralrio, A. Espinoza Vázquez, Plant extracts as green corrosion inhibitors for different metal surfaces and corrosive media: a review. *Processes* 8 (2020) 942. DOI: 10.3390/pr8080942

[23]. B. Sanyal, Organic compounds as corrosion inhibitors in different environments — a review. *Prog. Org. Coat.* 9 (1981) 165-236. DOI: 10.1016/0033-0655(81)80009-X

[24]. M.A. Ameer, A.M. Fekry, Corrosion inhibition of mild steel by natural product compound. *Prog. Org. Coat.* 71 (2011) 343-349. DOI: 10.1016/j.porgcoat.2011.04.001

[25]. A.J. Amalraj, J.W. Sahayaraj, A.P.P. Regis, A. Sahayaraj, P. Pandian, P. Johnraj, C. Kumar, Synergistic effect of Allium cepa-Zn^{2+} system on the corrosion of carbon steel in ground water. *Engineering* 5 (2013) 178-183. DOI: 10.4236/eng.2013.52025

[26]. H. Beddiar, S. Boudiba, M. Benahmed, A.N. Tamfu, Ö. Ceylan, K. Hanini, R.M. Dinica, Chemical composition, anti-quorum sensing, enzyme inhibitory, and antioxidant properties of phenolic extracts of *Clinopodium nepeta* L. Kuntze. *Plants* 10 (2021) 1955. DOI: 10.3390/plants10091955

[27]. C. Zeng, Z.Y. Zhou, W.J. Mai, Q.H. Chen, J.B. He, B.K. Liao, Exploration on the corrosion inhibition performance of Salvia miltiorrhiza extract as a green corrosion inhibitor for Q235 steel in HCl environment. *J. Mater. Res. Technol.* 32 (2024) 3857-3870. DOI: 10.1016/j.jmrt.2024.09.003

[28]. A.I. Kuruppu, P. Paranagama, C.L. Goonasekara, Medicinal plants commonly used against cancer in traditional medicine formulae in Sri Lanka. *Saudi Pharm. J.* 27 (2019) 565-573. DOI: 10.1016/j.jsps.2019.02.004

[29]. Ö.T. Erdogrul, Antibacterial activities of some plant extracts used in folk medicine. *Pharm. Biol.* 40 (2002) 269-273. DOI: 10.1076/phbi.40.4.269.8474

[30]. J. Lee, S. Noh, S. Lim, B. Kim, Plant extracts for type 2 diabetes: From traditional medicine to modern drug discovery. *Antioxidants* 10 (2021) 81. DOI: 10.3390/antiox10010081

[31]. B.E. Amitha Rani, B.B.J. Basu, Green inhibitors for corrosion protection of metals and alloys: an overview. *Int. J. Corros.* 2012 (2011) 380217. DOI: 10.1155/2012/380217

[32]. C.A. Loto, R.T. Loto, Effects of Nicotiana tobaccum extract additive on the quality of electroplating of zinc on mild steel. *Pol. J. Chem. Technol.* 15 (2013). DOI: 10.2478/pjct-2013-0008

[33]. R.T. Loto, C.A. Loto, M. Akinyele, Effect of

ginger, pomegranate and celery extracts on zinc electrodeposition, surface morphology and corrosion inhibition of mild steel. *Alex. Eng. J.* 59 (2020) 933-941. DOI: 10.1016/j.aej.2020.03.014

[34]. C.A. Loto, A. Olofinjana, J.E. Oniso, A.P.I. Popoola, Effect of Allium cepa (onion) extract additive on the morphology of zinc electroplated mild steel in acid chloride solution. *Can. J. Pure Appl. Sci.* 9 (2015) 3267-3277.

[35]. C.A. Loto, A. Olofinjana, R.T. Loto, Effect of *Manihot esculenta* C. leaf extract additive on the zinc electroplating on mild steel in acid chloride solution. *Int. J. Electrochem. Sci.* 9 (2014) 3746-3759. DOI: 10.1016/S1452-3981(23)08047-1

[36]. K. Hanini, S. Boudiba, B. Berka, L. Boudiba, S. Hioun, H. Beddiar, M. Benahmed, Corrosion inhibition impact of Pyracantha coccinea M. Roem extracts and their use as additives in zinc electroplating: Coating morphology, electrochemical and weight loss investigations, *J. Taiwan Inst. Chem. Engrs.* 121 (2021) 337-348. DOI: 10.1016/j.jtice.2021.04.007

[37]. E.E. Oguzie, Evaluation of the inhibitive effect of some plant extracts on the acid corrosion of mild steel. *Corros. Sci.* 50 (2008) 2993-2998. DOI: 10.1016/j.corsci.2008.08.004

[38]. S. Boudiba, K. Hanini, I. Selatnia, A. Saouane, S. Hioun, M. Benahmed, Experimental, theoretical and mathematical studies of *Echium italicum* L. extract as a corrosion inhibitor for carbon steel in acidic medium. *Mater. Res. Express* 6 (2019) 086546. DOI: 10.1088/2053-1591/ab194f

[39]. S. Akkal, F. Benayache, A. Bentamene, K. Medjroubi, E. Seguin, F. Tillequin, Flavonoid aglycones from *Centaurea napifolia*. *Chem. Nat. Compd.* 39 (2003) 219-220. DOI: 10.1023/A:1024834518756

[40]. M. Bruno, C. Fazio, M.P. Paternostro, J.G. Díaz, W. Herz, *Sesquiterpene lactones* and other constituents of *Centaurea napifolia*. *Planta Med*. 61 (1995) 374-375. DOI: 10.1055/s-2006-958108

[41]. F. Senatore, D. Rigano, R. De Fusco, M. Bruno, Volatile components of *Centaurea cineraria* L. subsp. *umbrosa* (Lacaita) Pign. and *Centaurea napifolia* L. (Asteraceae), two species growing wild in Sicily. *Flavour Fragr. J.* 18 (2003) 248-251. DOI: 10.1002/ffj.1179

[42]. M. Benahmed, N. Djeddi, S. Akkal, H. Laouar, *Saccocalyx satureioides* as corrosion inhibitor for carbon steel in acid solution. *Int. J. Ind. Chem.*, 7 (2016) 109-120. DOI: 10.1007/s40090-016-0082-z

[43]. C.A. Loto, R.T. Loto, Effect of dextrin and thiourea additives on the zinc electroplated mild steel in acid chloride solution. *Int. J. Electrochem. Sci.* 8 (2013) 12434-12450. DOI: 10.1016/S1452-3981(23)13278-0

[44]. C.A. Loto, Synergism of *Saccharum officinarum* and *Ananas comosus* extract additives on the quality of electroplated zinc on mild steel. *Res. Chem. Intermed.* 40 (2014) 1799-1813. DOI: 10.1007/s11164-013-1083-6

[45]. D. ASTM, 3359-02: standard test methods for measuring adhesion by tape test. ASTM International, West Conshohocken, PA, 2002.

[46]. L. Guo, B. Tan, W. Li, Q. Li, X. Zheng, I.B. Obot, *Banana* leaves water extracts as inhibitor for X70 steel corrosion in HCl medium. *J. Mol. Liq.* 327 (2021) 114828. DOI: 10.1016/j.molliq.2020.114828

[47]. P. Muthukrishnan, K. Saravana Kumar, B. Jeyaprabha, P. Prakash, Anticorrosive activity of *Kigelia pinnata* leaves extract on mild steel in acidic media. *Metall. Mater. Trans. A* 45 (2014) 4510-4524. DOI: 10.1007/s11661-014-2366-2

[48]. A. El Bribri, M. Tabyaoui, B. Tabyaoui, H. El Attari, F. Bentiss, The use of *Euphorbia falcata* extract as eco-friendly corrosion inhibitor of carbon steel in hydrochloric acid solution. *Mater. Chem. Phys.* 141 (2013) 240-247. DOI: 10.1016/j.matchemphys.2013.05.006

[49]. P. Nath, D.K. Sahu, A. Mallik, Physicochemical and corrosion properties of sono-electrodeposited Cu-Ni thin films. *Surf. Coat. Technol.* 307 (2016) 772-780. DOI: 10.1016/j.surfcoat.2016.09.085

[50]. I.M. Omar, A.M. Al-Fakih, Effect of red clover (*Trifolium pratense* L.) aqueous extract as an additive on nickel electrodeposition: Experimental and theoretical study. *Arab. J. Chem*. 17 (2024) 105680. DOI: 10.1016/j.arabjc.2024.105680

[51]. G. Fabricius, G. Sundholm, The effect of additives on the electrodeposition of copper studied by the impedance technique. *J. Appl. Electrochem.* 14 (1984) 797-801. DOI: 10.1007/BF00615270

[52]. R.K. Shervedani, A.R. Madram, Kinetics of hydrogen evolution reaction on nanocrystalline electrodeposited $Ni_{62}Fe_{35}C_3$ cathode in alkaline solution by electrochemical impedance spectroscopy. *Electrochim. Acta* 53 (2007) 426-433. DOI: 10.1016/j.electacta.2007.06.006

[53]. A. Yurt, S. Ulutas, H. Dal, Electrochemical and theoretical investigation on the corrosion of aluminium in acidic solution containing some Schiff bases. *Appl. Surf. Sci.* 253 (2006) 919-925. DOI: 10.1016/j.apsusc.2006.01.026

[54]. T.K. Rout, Electrochemical impedance spectroscopy study on multi-layered coated steel sheets. *Corros. Sci.* 49 (2007) 794-817. DOI: 10.1016/j.corsci.2006.06.008

[55]. Anchors, H.E., Anchor bolt and sleeve assembly of material indicated below with capability to sustain, without failure, a load equal to 6 times the load imposed when installed in unit masonry assemblies and equal to 4 times the load imposed when

installed in concrete as determined by testing per ASTM E 488 conducted by a qualified independent testing and inspecting agency. 1. Material: Carbon-steel components, zinc plated to comply with ASTM B, 2010. 633: p. 061053-6.

[56]. D. ASTM, A879-Steel Sheet. Zinc Coated by the Electrolytic Process for Applications Requiring Designation of the Coating Mass on Each Surface. IHS Markit Standards Store, 2012.

[57]. ISO 2813:2014, Paints and varnishes — Determination of gloss value at 20°, 60° and 85°.

[58]. D. ASTM, 523-89, Standard Test Method for Specular Gloss. ASTM International, 1999.

[59]. X. Li, S. Deng, H. Fu, Adsorption and inhibition effect of vanillin on cold rolled steel in 3.0M H_3PO_4. *Prog. Org. Coat.* 67 (2010) 420-426. DOI: 10.1016/j.porgcoat.2009.12.006

[60]. D.K. Lavanya, V.P. Frank, D.P. Vijaya, S. Bangera, Inhibition effect of thiourea derivative for mild steel corrosion in acid medium: experimental and theoretical studies. *J. Bio- Tribo-Corros.* 7 (2021) 47. DOI: 10.1007/s40735-021-00487-7

[61]. A. Zarrouk, B. Hammouti, T. Lakhlifi, M. Traisnel, H. Vezin, F. Bentiss, New 1H-pyrrole-2,5-dione derivatives as efficient organic inhibitors of carbon steel corrosion in hydrochloric acid medium: electrochemical, XPS and DFT studies. *Corros. Sci.* 90 (2015) 572-584. DOI: 10.1016/j.corsci.2014.10.052

[62]. C.B. Verma, M.A. Quraishi, A. Singh, 2-Aminobenzene-1,3-dicarbonitriles as green corrosion inhibitor for mild steel in 1 M HCl: Electrochemical, thermodynamic, surface and quantum chemical investigation. *J. Taiwan Inst. Chem. Eng.* 49 (2015) 229-239. DOI: 10.1016/j.jtice.2014.11.029

[63]. S. Saravanamoorthy, S. Velmathi, Physiochemical interactions of chiral Schiff bases on high carbon steel surface: Corrosion inhibition in acidic media. *Prog. Org. Coat.* 76 (2013) 1527-1535. DOI: 10.1016/j.porgcoat.2013.06.003

[64]. X. Li, S. Deng, H. Fu, X. Xie, Synergistic inhibition effects of bamboo leaf extract/major components and iodide ion on the corrosion of steel in H_3PO_4 solution. *Corros. Sci.* 78 (2014) 29-42. DOI: 10.1016/j.corsci.2013.08.025

[65]. E. Berdimurodov, A. Kholikov, K. Akbarov, I.B. Obot, L. Guo, Thioglycoluril derivative as a new and effective corrosion inhibitor for low carbon steel in a 1 M HCl medium: Experimental and theoretical investigation. *J. Mol. Struct.* 1234 (2021) 130165. DOI: 10.1016/j.molstruc.2021.130165

[66]. N. Mechbal, M.E. Belghiti, N. Benzbiria, C.H. Lai, Y. Kaddouri, Y. Karzazi, M. Zertoubi, Correlation between corrosion inhibition efficiency in sulfuric acid medium and the molecular structures of two newly eco-friendly pyrazole derivatives on iron oxide surface. *J. Mol. Liq.* 331 (2021) 115656. DOI: 10.1016/j.molliq.2021.115656

[67]. A.O. James, N.B. Iroha, New green inhibitor of Olax subscorpioidea root for J55 carbon steel corrosion in 15% HCl: theoretical, electrochemical, and surface morphological investigation. *Emerg. Mater.* 5 (2022) 1119-1131. DOI: 10.1007/s42247-021-00161-1

[68]. N.R.J. Hynes, R.M. Selvaraj, T. Mohamed, A.M. Mukesh, O. Karoui, M.P. Nikolova, *Aerva lanata* flowers extract as green corrosion inhibitor of low-carbon steel in HCl solution: an in vitro study. *Chem. Pap.* 75 (2021) 1165-1174. DOI: 10.1007/s11696-020-01361-5

[69]. M.V.L. da Silva, E. de Britto Policarpi, A. Spinelli, Syzygium cumini leaf extract as an eco-friendly corrosion inhibitor for carbon steel in acidic medium. *J. Taiwan Inst. Chem. Eng*. 129 (2021) 342-349. DOI: 10.1016/j.jtice.2021.09.026

[70]. K. Hjouji, E. Ech-chihbi, I. Atemni, M. Ouakki, T. Ainane, M. Taleb, Z. Rais, Datura stramonium plant seed extracts as a new green corrosion inhibitor for mild steel in 1M HCl solution: Experimental and surface characterization studies. *Sustain. Chem. Pharm.* 34 (2023) 101170. DOI: 10.1016/j.scp.2023.101170

[71]. M.H. Hussin, M.J. Kassim, The corrosion inhibition and adsorption behavior of Uncaria gambir extract on mild steel in 1 M HCl. *Mater. Chem. Phys*. 125 (2011) 461-468. DOI: 10.1016/j.matchemphys.2010.10.032

[72]. O.A. Akinbulumo, O.J. Odejobi, E.L. Odekanle, Thermodynamics and adsorption study of the corrosion inhibition of mild steel by *Euphorbia heterophylla* L. extract in 1.5 M HCl. *Results Mater.* 5 (2020) 100074. DOI: 10.1016/j.rinma.2020.100074

[73]. N. Djeddi, M. Benahmed, S. Akkal, H. Laouer, E. Makhloufi, N. Gherraf, Study on methylene dichloride and butanolic extracts of *Reutera lutea* (Desf.) Maire (Apiaceae) as effective corrosion inhibitors for carbon steel in HCl solution. *Res. Chem. Intermed.* 41 (2015) 4595-4616. DOI: 10.1007/s11164-014-1555-3

[74]. C.P. Kumar, K.N. Mohana, Corrosion inhibition efficiency and adsorption characteristics of some Schiff bases at mild steel/hydrochloric acid interface. *J. Taiwan Inst. Chem. Eng.* 45 (2014) 1031-1042. DOI: 10.1016/j.jtice.2013.08.017

[75]. E. Oguzie, C.K. Enenebeaku, C.O. Akalezi, et al., Adsorption and corrosion-inhibiting effect of *Dacryodis edulis* extract on low-carbon-steel corrosion in acidic media. *J. Colloid Interface Sci.* 349 (2010) 283-292. DOI: 10.1016/j.jcis.2010.05.027

[76]. A. Kosari, M.H. Moayed, A. Davoodi, R. Parvizi, M. Momeni, H. Eshghi, H. Moradi, Electrochemical

and quantum chemical assessment of two organic compounds from pyridine derivatives as corrosion inhibitors for mild steel in HCl solution under stagnant condition and hydrodynamic flow. *Corros. Sci*. 78 (2014) 138-150. DOI: 10.1016/j.corsci.2013.09.009

[77]. H. Mahfoud, N. Rouag, S. Boudiba, M. Benahmed, K. Morakchi, S. Akkal, Mathematical and electrochemical investigation of *Lamium flexuosum* extract as effective corrosion inhibitor for CS in acidic solution using multidimensional minimization program system. *Arab. J. Sci. Eng.* 47 (2022) 6605-6616. DOI: 10.1007/s13369-021-06546-y

[78]. X. Li, S. Deng, H. Fu, Inhibition of the corrosion of steel in HCl, H_2SO_4 solutions by bamboo leaf extract. *Corros. Sci.* 62 (2012) 163-175. DOI: 10.1016/j.corsci.2012.05.008

[79]. P. Muthukrishnan, B. Jeyaprabha, P. Prakash, Adsorption and corrosion inhibiting behavior of *Lannea coromandelica* leaf extract on mild steel corrosion. *Arab. J. Chem*. 10 (2017) S2343-S2354. DOI: 10.1016/j.arabjc.2013.08.011

[80]. L. Li, X. Zhang, J. Lei, J. He, S. Zhang, F. Pan, Adsorption and corrosion inhibition of *Osmanthus fragran* leaves extract on carbon steel. *Corros. Sci*. 63 (2012) 82-90. DOI: 10.1016/j.corsci.2012.05.026

[81]. S.A. Umoren, U.M. Eduok, M.M. Solomon, A.P. Udoh, Corrosion inhibition by leaves and stem extracts of *Sida acuta* for mild steel in 1 M H_2SO_4 solutions investigated by chemical and spectroscopic techniques. *Arab. J. Chem*. 9 (2016) S209-S224. DOI: 10.1016/j.arabjc.2011.03.008

[82]. K. Tebbji, N. Faska, A. Tounsi, H. Oudda, M. Benkaddour, B. Hammouti, The effect of some lactones as inhibitors for the corrosion of mild steel in 1 M hydrochloric acid. *Mater. Chem. Phys.* 106 (2007) 260-267. DOI: 10.1016/j.matchemphys.2007.05.046

[83]. X. Li, S. Deng, H. Fu, T. Li, Adsorption and inhibition effect of 6-benzylaminopurine on cold rolled steel in 1.0 M HCl. *Electrochim. Acta* 54 (2009) 4089-4098. DOI: 10.1016/j.electacta.2009.02.084

[84]. X. Li, S. Deng, H. Fu, G. Mu, Synergistic inhibition effect of rare earth cerium (IV) ion and anionic surfactant on the corrosion of cold rolled steel in H_2SO_4 solution. *Corros. Sci.* 50 (2008) 2635-2645. DOI: 10.1016/j.corsci.2008.06.026

[85]. L. Bammou, M. Belkhaouda, R. Salghi, et al., Corrosion inhibition of steel in sulfuric acidic solution by the Chenopodium ambrosioides extracts. *J. Assoc. Arab Univ. Basic Appl. Sci.* 16 (2014) 83-90. DOI: 10.1016/j.jaubas.2013.11.001

[86]. M.N. El-Haddad, Hydroxyethylcellulose used as an eco-friendly inhibitor for 1018 C-steel corrosion in 3.5% NaCl solution. *Carbohydr. Polym*. 112 (2014) 595-602. DOI: 10.1016/j.carbpol.2014.06.032

[87]. Y. El Ouadi, A. Bouyanzer, L. Majidi, J. Paolini, J.M. Desjobert, J. Costa, T. Ben Hadda, Evaluation of Pelargonium extract and oil as eco-friendly corrosion inhibitor for steel in acidic chloride solutions and pharmacological properties. *Res. Chem. Intermed*. 41 (2015) 7125-7149. DOI: 10.1007/s11164-014-1802-7

[88]. S. Martinez, I. Stern, Thermodynamic characterization of metal dissolution and inhibitor adsorption processes in the low carbon steel/mimosa tannin/sulfuric acid system. *Appl. Surf. Sci.* 199 (2002) 83-89. DOI: 10.1016/S0169-4332(02)00546-9

[89]. I.E. Uwah, P.C. Okafor, V.E. Ebiekpe, Inhibitive action of ethanol extracts from Nauclea latifolia on the corrosion of mild steel in H_2SO_4 solutions and their adsorption characteristics. *Arab. J. Chem*. 6 (2013) 285-293. DOI: 10.1016/j.arabjc.2010.10.008

[90]. M. Behpour, S.M. Ghoreishi, M. Khayatkashani, N. Soltani, Green approach to corrosion inhibition of mild steel in two acidic solutions by the extract of Punica granatum peel and main constituents. *Mater. Chem. Phys.* 131 (2012) 621-633. DOI: 10.1016/j.matchemphys.2011.10.027

[91]. H. Zarrok, A. Zarrouk, B. Hammouti, R. Salghi, C. Jama, F. Bentiss, Corrosion control of carbon steel in phosphoric acid by purpald-eight loss, electrochemical and XPS studies. *Corros. Sci.* 64 (2012) 243-252. DOI: 10.1016/j.corsci.2012.07.018

[92]. E.B. Caldona, M. Zhang, G. Liang, et al., Corrosion inhibition of mild steel in acidic medium by simple azole-based aromatic compounds. *J. Electroanal. Chem.* 880 (2021) 114858. DOI: 10.1016/j.jelechem.2020.114858

[93]. E. Ech-Chihbi, A. Nahlé, R. Salim, F. Benhiba, A. Moussaif, F. El-Hajjaji, A. Zarrouk, Computational, MD simulation, SEM/EDX and experimental studies for understanding adsorption of benzimidazole derivatives as corrosion inhibitors in 1.0 M HCl solution. *J. Alloys Compd.* 844 (2020) 155842. DOI: 10.1016/j.jallcom.2020.155842

[94]. R. Yıldız, An electrochemical and theoretical evaluation of 4,6-diamino-2-pyrimidinethiol as a corrosion inhibitor for mild steel in HCl solutions. *Corros. Sci.* 90 (2015) 544-553. DOI: 10.1016/j.corsci.2014.10.047

[95]. S. Deng, X. Li, Inhibition by Ginkgo leaves extract of the corrosion of steel in HCl and H_2SO_4 solutions. *Corros. Sci.* 55 (2012) 407-415. DOI: 10.1016/j.corsci.2011.11.005

[96]. H.M. Abd El-Lateef, Experimental and computational investigation on the corrosion inhibition characteristics of mild steel by some novel synthesized imines in hydrochloric acid solutions. *Corros. Sci.* 92 (2015) 104-117. DOI: 10.1016/j.corsci.2014.11.040

[97]. H. Soltani, K. Hanini, M. Benahmed, S. Boudiba, L. Boudiba, A.N. Tamfu, A .Zellagui, S. Akkal. Investigating Centaurea napifolia Extracts for Zinc Electroplating Efficiency and Corrosion Prevention: Experimental and Surface Analysis. This preprint has been posted on Research Square. (Version 1), 2024. DOI: 10.21203/rs.3.rs-4232896/v1